

BUNDESANSTALT FÜR GEOWISSENSCHAFTEN UND ROHSTOFFE
HANNOVER



TIPTEQ-Teilvorhaben : Seismoturbidite

BMBF-Forschungsvorhaben 03G0595A

Fachlicher Abschlussbericht
Projektlaufzeit 01.01.2004 – 30.06.2005

1. Sachbearbeiter: Dr. M. Wiedicke (Projektleiter), Dr. T. Reichel
2. Auftraggeber: Bundesministerium für Bildung, Wissenschaft, Forschung und Technologie (FV 03G0595A), Projektträger Jülich
3. Datum: Dezember 2005

Inhaltsangabe

	Seite
1. Fragestellung	3
2. Durchführung des Vorhabens (Geländearbeit, Ablauf, durchgeführte Untersuchungen etc.)	3
3. Kooperation	5
4. Wissenschaftliche Ergebnisse	5
5. Literaturverzeichnis	10
6. Dank	11
Erfolgskontrollbericht	12

ANNEX

A – 1: Liste der Vorträge und Poster	13
A – 2: Manuskript Reichel, Wiedicke et al.	14ff
A – 3: Berichtsblatt / Document Control Sheet	

Das diesem Bericht zugrundeliegende Vorhaben wurde mit Mitteln des Bundesministeriums für Bildung, und Forschung unter dem Förderkennzeichen FV 03G0595A. gefördert. Die Verantwortung für den Inhalt dieser Veröffentlichung liegt beim Autor.

Das Vorhaben „Seismoturbidite“ ist Teil des Teilprojektes TIPTEQ 5 „Koseismische Massenumlagerungen und Oberflächenprozesse“ des Verbundvorhabens „TIPTEQ [from The Incoming Plate to mega-Thrust EarthQuake processes]“, welches im Rahmen des BMBF/DFG-Förderprogramm GEOTECHNOLOGIEN „Kontinentränder – Brennpunkte im Nutzungs- und Gefährdungspotenzial durchgeführt wurde.

1. Fragestellung

Seismoturbidite – durch Starkbeben ausgelöste submarine Massenumlagerungen.

Das Teilprojekt „Koseismische Massenumlagerung“, in das die Thematik Seismoturbidite eingebettet ist, befasst sich mit unterschiedlichen Formen fossiler Massenumlagerungen, die durch Starkbeben ausgelöst worden sind. Durch Untersuchung von Merkmalen wie Topographie und Lithologie/Sedimentologie sowie Alter und geographische Ausdehnung werden unterschiedliche Typen von Massenumlagerungen charakterisiert. Die Untersuchungen dienen der Ermittlung indirekter Indikatoren seismischer Aktivität; diese ergänzen bzw. erweitern den limitierten Kenntnisstand über Starkbeben, der aus direkten seismischen Messungen und gesicherten historischen Beschreibungen zusammengetragen wurde.

Das Vorhaben „Seismoturbidite“ zielte auf die Erfassung submariner Indikatoren für Paläoseismizität. Massenumlagerungen wie submarine Hangrutschungen oder Trübe-stromablagerungen sollten identifiziert und datiert werden, und mittels ihrer Ausdehnung auf einen Zusammenhang mit Bebenaktivität untersucht werden. Ziel war die Ermittlung quartärer bzw. holozäner Rekurrenzraten für Starkbeben in Südchile. Die Ergebnisse dienen dazu, das aus Starkbeben resultierende Gefährdungspotenzial und die Gefährdungsverteilung besser zu verstehen.

2. Durchführung des Vorhabens

Feldarbeiten:

Proben- und Datenmaterial, welches für die Untersuchungen herangezogen wurde, war während einer Kampagne von FS SONNE vor Südchile im Jahr 2002 (SO161-Leg 5, 24.12.2001 – 26.01.2002, SPOC) gewonnen worden. Daher konzentrierten sich die Projektaktivitäten auf die Bearbeitung, Sichtung und Auswertung von SO161-Daten und Kernmaterial.

Zeitplan:

Der ursprüngliche Finanzierungs- und Zeitplan sah als Beginn der Projektarbeiten den 1.1.2004 vor. Da aber nach der Bewilligung für die Arbeiten zunächst ein wissenschaftlicher Projektmitarbeiter ausgewählt und eingestellt werden musste, wurde der Projektbeginn um 4 Monate auf den 1. Mai 2004 verschoben. Das Vorhaben endete am 30. Juni 2005.

Zunächst wurden Sedimentkerne der SO161-5 Kampagne gesichtet und auf ihre Eignung für die Fragestellung geprüft. Insbesondere sollten Umlagerungereignisse identifiziert und beschrieben werden. Es wurden 6 Kerne aus Hangbecken und dem

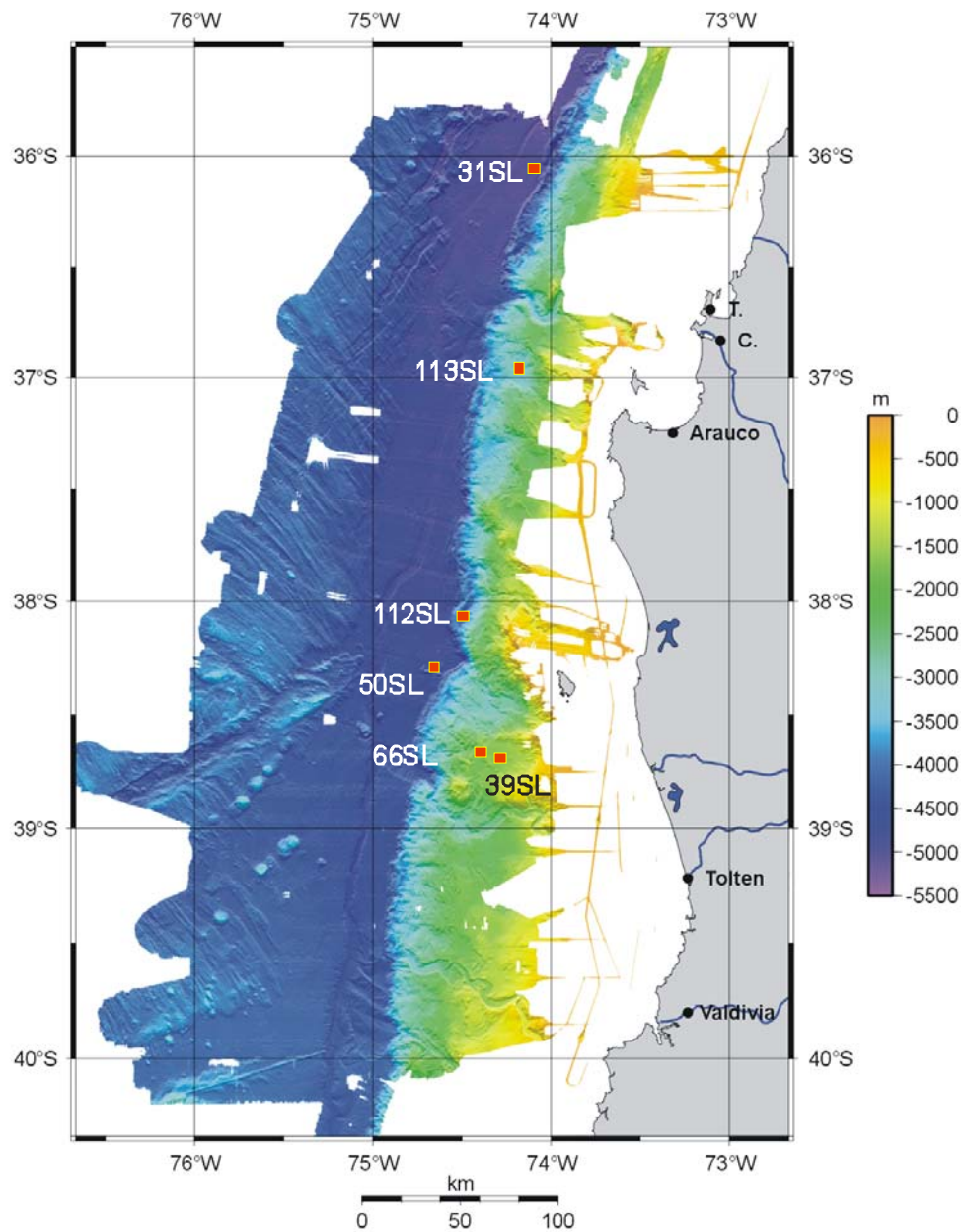


Abb. 1: Bathymetrische Karte des südchilenischen Kontinentrandes mit der Lage der 6 Kernpositionen dieser Studie.

Tiefseegraben vor S-Chile ausgewählt und sedimentologisch charakterisiert. Für die Auswahl wurden auch die während SO161-5 akquirierten hochauflösenden Parasound-Profile (sofern sie bei dem steilen Terrain aussagekräftig waren) herangezogen. Von den wichtigsten Kernen wurden dünne vertikal angeordnete Sedimentscheiben entnommen, um Radiographien anzufertigen; sie erfassen Details der Strukturen der Sedimentsequenz. Die Kerne wurden in 10cm-Intervallen für die Erstellung stabiler Sauerstoff-Isotopenkurven beprobt. Für ausgewählte Kerne wurden chemische Analysen (RFA) der

Sedimentfolge durchgeführt. Von allen Kernen wurde mit Hilfe des ‚Spectrolino‘-Geräts je ein hochauflösendes vertikales Farbprofil erstellt. Es gestattet in Kombination mit Daten des Multi-Sensor-Core-Loggers und den Radiographien eine differenzierte Charakterisierung der sedimentologischen Einheiten der Kerne.

In der zweiten Phase wurden die aussagekräftigsten Kerne bestimmt, an denen AMS¹⁴C- sowie ²¹⁰Pb-Analysen durchgeführt wurden, um absolute Alter zu erhalten und damit möglichst differenzierte Altersmodelle für die Kerne erstellen zu können.

Die ersten Ergebnisse wurden von Herrn Reichel auf der AGU-Tagung, 13.-18. Dezember 2004, in San Francisco vorgestellt sowie auf dem SONNE-Statusseminar, 9.-11.3.2005 in Warnemünde. Eine Zusammenfassung der Ergebnisse präsentierte Herr Wiedicke auf dem Statusseminar Kontinentränder, 9.-10. Juni 2005 in Potsdam. Die Ergebnisse sind im nachfolgenden Kapitel 4 zusammengefasst sowie in den beigefügten Publikationsmanuskripten (siehe Anlagen ANNEX A-2).

3. Kooperation

Die Beprobungskampagne mit FS SONNE (SO161-5, SPOC) wurde in enger Kooperation mit deutschen und chilenischen Partnern durchgeführt:

- GEOMAR, Kiel
- SFB 267 der DFG (Deformation Processes in the Andes)
- GFZ Potsdam
- Freie Universität, Berlin
- Empresa Nacional del Petroleo, Santiago de Chile
- Servicio Nacional de Geología y Minería (SERNAGEOMIN), Santiago de Chile
- Servicio de Hidrografía y Oceanografía de la Armada (SHOA), Santiago de Chile
- Universidad de Chile, Santiago de Chile
- Universidad Católica de Valparaíso
- Universidad de Concepción
- Instituto Geográfico Militar (IGM), Santiago de Chile
- Servicios Geofísicos en Minería e Ingeniería (SEGMI), Santiago de Chile

Die Auswertearbeiten erfolgten in Zusammenarbeit mit Kollegen folgender Partner:

- GFZ Potsdam
- Universität Mainz
- Universität Bremen
- Verbundpartnern TIPTEQ 5 (Univ.Potsdam, GFZ)

4. Wissenschaftlich-technische Ergebnisse

Der Zusammenhang zwischen submarinen Massenumlagerungen und Erdbeben ist seit langem bekannt; ein eindrucksvolles Fallbeispiel wird von Heezen & Ewing (1952) von der kanadischen Atlantikküste beschrieben. Da Massenumlagerungen und Turbidite

zahlreiche Ursachen haben können, liegen hinsichtlich der Erforschung in jünger Zeit die Akzente in der Differenzierung von Kriterien und in der Herstellung von präzisen zeitlichen Korrelationen zu historisch bekannten seismischen Ereignissen (Adams 1990; Anastasakis and Piper, 1991; Grantz et al., 1996; Nakajima and Kanai, 2000; Blais-Stevens & Clague, 2001; und andere). Als wichtigste Kriterien sind demnach die gute zeitlich Einordnung von Umlagerungseignissen und die grosse Ausdehnung bzw. geographische Verbreitung von einzelnen sedimentären ‚Events‘ zu nennen (z.B. Goldfinger et al, 2003). Für die Korrelation mit Starkbeben haben wir die Auflistungen von chilenischen Beben in den Publikationen von Lomnitz (1970) und Cifuentes (1989) herangezogen.

Für die vorliegende Studie wurden erfolgreich mehrere Hangbecken und der Tiefseegraben vor S-Chile beprobt und in den gewonnenen Kernen zahlreiche Umlagerungs-Lagen identifiziert. Die genannte topographische Differenzierung bei der Probennahme ist wichtig, um lokale von regionalen Ereignissen unterscheiden zu können: die Kerne 39SL, 66SL 112SL und 113SL aus Hangbecken liefern primär lokale Informationen, während die Grabenpositionen 31SL, 33SL und 50SL regionale Einzugsgebiete besitzen. Als Beispiel sei hier Kern 112SL gezeigt, dessen Beckenposition einen benachbarten steilen Hang von mehr als 170 km^2 mit Hangneigungen von 20° als Einzugsgebiet aufweist (Abb. 2); gegenüber dem Tiefseegraben ist er durch eine morphologische Barriere abgeschirmt. Er weist acht mächtige Turbiditlagen auf, die sedimentologisch mit Hilfe von Radiographien, Kernlogger und Farbprofil gut identifiziert werden können.

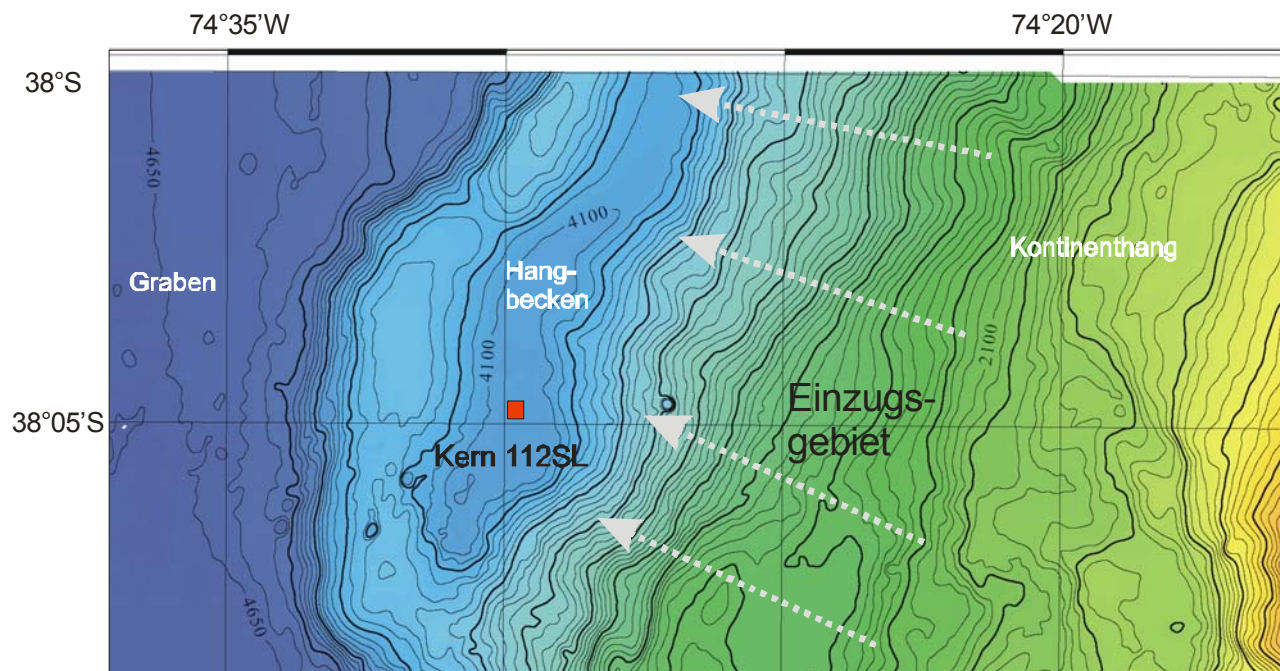


Abb. 2: Bathymetrische Karte des Beckens am Fuss des Kontinentalhangs mit der Position des Kerns 112SL. Das Hangbecken befindet sich am Fuss eines steilen langen Hanges, der als riesiges Einzugsgebiet für Hangrutschungen wirkt Vom Tiefseegraben ist das Becken durch eine Barriere abgeschirmt (50 m - Kontourlinien)

Die stratigraphische Einstufung der Kerne wurde mit Hilfe der Analyse stabiler Sauerstoffisotope durchgeführt (Abb. 3) und anschliessend mit AMS¹⁴C-Datierungen verifiziert und präzisiert.

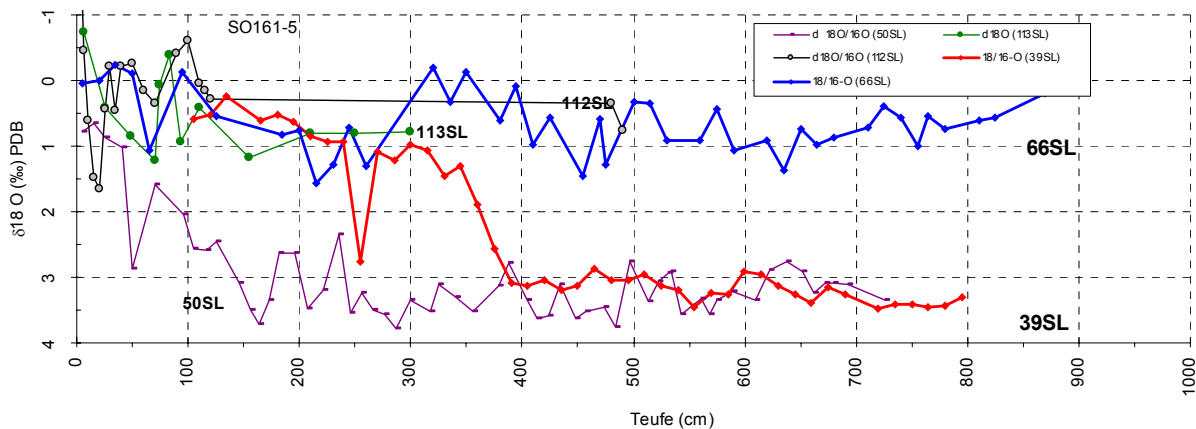


Abb. 3: Stabile Sauerstoff-Isotopenkurven für die Kerne 31SL, 39SL, 50SL, 66SL, 112SL und 113SL. Das holozäne $\delta^{18}\text{O}$ -Niveau liegt bei etwa 0 - 1 ‰ (PDB), das glaziale Niveau bei etwa 2,5 - 3,5 ‰ (PDB) (=> Beispiel: Kern 66SL (blaue Kurve) bleibt durchgehend auf dem „leichten“ Niveau von 0-1 ‰ (PDB) und besteht demnach bis zur Basis (knapp 9 m) aus holozänen Ablagerungen; demgegenüber repräsentiert der Abschnitt 4 - 8 m des Kern 39SL (rote Kurve) pleistozäne Sedimente).

Die wichtigsten Ergebnisse aus den stratigraphischen Untersuchungsgängen sind:

- Kerne, die aus Hangbecken mit grossem Einzugsbereich (=>Sedimentfallen) stammen - wie 66SL, 112SL und 113SL - zeigen sehr hohe Sedimentationsraten von 300 cm/1000 J. bis zu 900 cm/1000 J. (in 112SL).
- Wegen des vergleichsweise hohen Sand-/Siltanteils sind Kerne aus dem Tiefseegraben meist recht kurz (geringe Eindringung des Kerngerätes) bzw. kaum datierbar. Zu letztgenanntem Problem trägt auch die grosse Wassertiefe von > 4200 m bei, in der Karbonat weggelöst wird (Ausnahmen bilden Kern 50SL sowie bedingt 31SL).
- in Kern 50SL zeigt sich eine deutliche Abnahme der Sedimentationsraten um mindestens eine Größenordnung vom Pleistozän zum Holozän: Während für das Pleistozän mehr als 100 cm/1000 J. ermittelt wurden sind es für das Holozän ca. 10 cm/1000 J.

Dadurch wird das Vorhaben der Korrelation von Kernen des Tiefseegrabens mit denjenigen der Hangbecken erschwert. Eine solche Korrelation von Kernen bzw. darin enthaltener Sedimentlagen stellt jedoch eine wichtige Absicherung der Deutung als seismisch bedingte Massenumlagerung dar.

Auf der Basis der erarbeiteten Altersmodelle lassen sich für die datierbaren Kerne mittlere Wiederholungsraten für Turbiditereignisse (bzw. Massenumlagerungen) bestimmen. Diese Rekurrenzraten liegen für die beiden Kerne der Hangbecken deutlich höher (rund 80-90 a) als für den Kern aus dem Tiefseegraben (290 a). Hier muss allerdings die Hochlage der Kernposition von 50SL berücksichtigt werden, die eine kondensierte Sedimentation bedingt. Daher erfasst diese Lokation nur besonders intensive Turbiditereignisse – sie besitzt somit ein geringeres zeitliches Auflösungsvermögen als die Hangpositionen. Gemäss den absoluten Altersdatierungen erfasst der Kern im Wesentlichen das jüngste Pleistozän, ist also auch hinsichtlich des repräsentierten Zeitabschnitts nicht mit den spätholozänen Sequenzen der Hangkerne direkt vergleichbar.

Die ermittelten Rekurrenzraten für Turbidite wurden dann mit Wiederholungsraten von Starkbeben aus historischer Zeit verglichen, die der Literatur entnommen wurden; ein solcher Vergleich sollte sich auf die Größenordnung der Werte beschränken, da vielfach in der Literatur die seismisch betroffene Zonen regional nicht präzise genug eingegrenzt wurden. Cifuentes (1989) gibt für Chile eine Rekurrenzrate von etwa 150 a an, nach Nishenko (1985) liegt sie in Südchile meist zwischen etwa 90 und 130a (13 -128a).

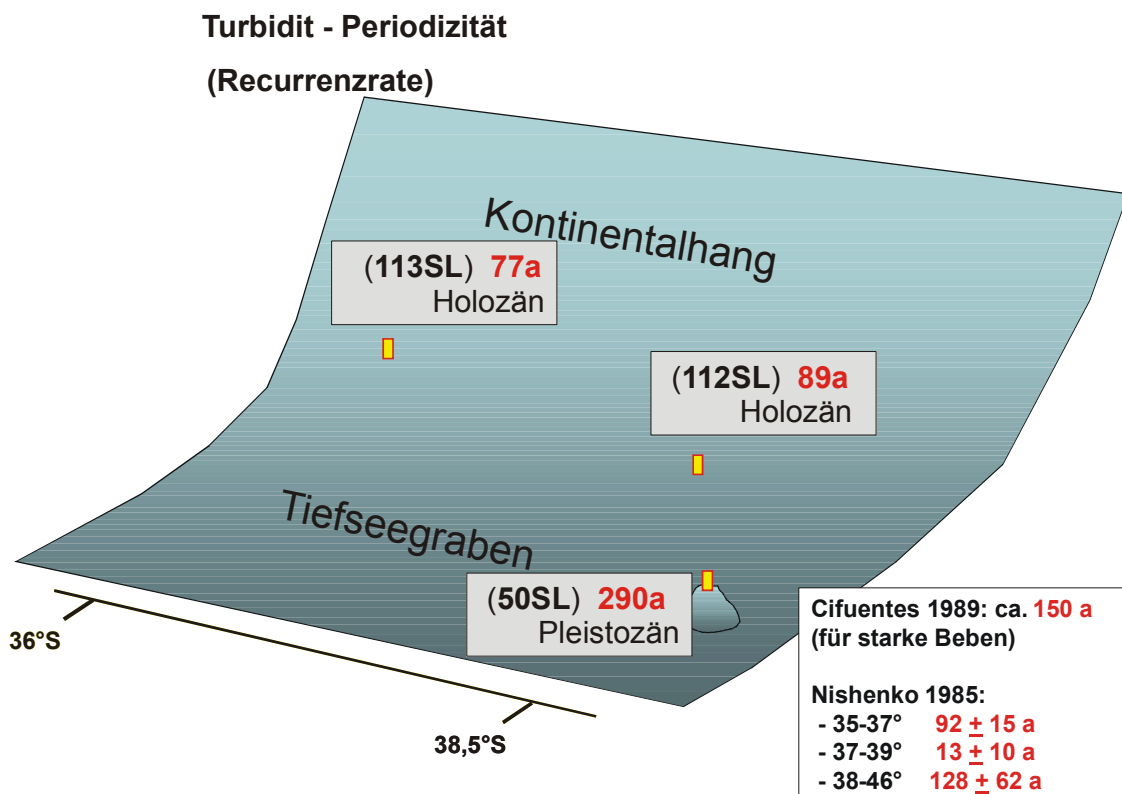


Abb. 4: Mittlere Wiederholungsraten für Umlagerungssereignisse von 3 Kernpositionen des chilenischen Kontinentalhangs und Tiefseegrabens.

Die von uns ermittelten Rekurrenzraten für Umlagerungssereignisse von rd. 80-90 a liegen in der gleichen Größenordnung wie diejenigen für Starkbeben in Chile in historischer Zeit. Da es sich bei diesen Werten um Mittelwerte handelt, ist eine zeitliche Korrelation der unterschiedlichen Ereignisse damit jedoch nicht belegt.

Am hochauflösenden Kern 112SL wurde diese Korrelation zwischen Beben und Umlagerungssereignissen geprüft (Abb. 5): Es gelang, die beiden tiefsten Turbidite des Kerns zu datieren. Basierend auf dieser Alterseinstufung korreliert die Anzahl der mächtigen Turbiditlagen recht gut mit den historisch nachgewiesenen Starkbeben, wenn als Äquivalent für die beiden seismischen Ereignispärchen 1570/75 und 1835/37 lediglich eine Turbiditlage angenommen wird. Diese Annahme erscheint durchaus plausibel, da wir davon ausgehen, dass mobilisierbares Sedimentmaterial in der kurzen Zeitspanne von 2 bzw. 5 Jahren nach einem grossen Ereignis nicht in ausreichendem Umfang akkumuliert werden konnte. Die Datierung mittels ^{210}Pb -Isotopie (auch noch unterhalb des obersten Turbidits nachgewiesen!) stützt diese Interpretation. Die absolute Datierung aller Einzellagen ist uns allerdings nicht gelungen, da nicht genug datierbares Material zwischen allen Turbiditlagen auszulesen war.

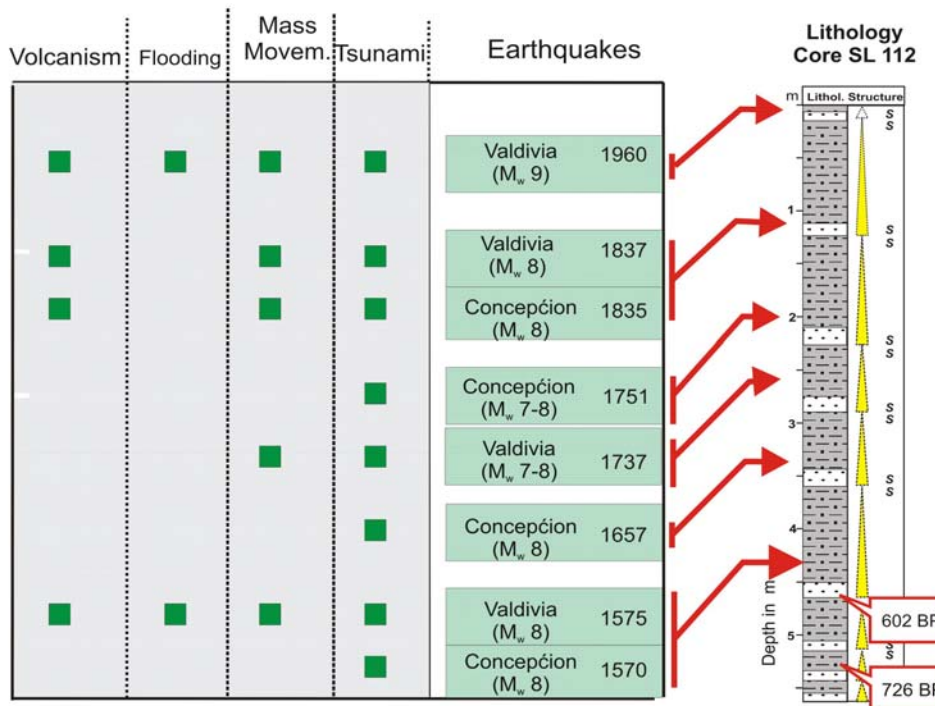


Abb. 5: Historische Starkbeben in Südkalifornien und ihre schädlichen Auswirkungen; die Anzahl der Turbiditlagen von Kern 112SL korreliert gut mit den wichtigen Starkbeben der vergangenen rd. 500 Jahre

Wir gehen daher davon aus, dass der von uns gewählte Ansatz, die Sedimentsequenz als Archiv für Paläoseismizität zu lesen, grundsätzlich und unter idealen Bedingungen anwendbar ist. Um zu spezifischen belastbareren Detailaussagen vor Chile zu gelangen, müssten aber weitere Kernpositionen analysiert / datiert werden, um eine Korrelation zwischen mehreren Hangbecken etablieren zu können. Eine Herausforderung bildet dabei die geringe Menge von datierbaren Sedimentkomponenten, die insbesondere die ¹⁴C-Datierungen betrifft.

5. Literatur

- Adams, J., 1990, Paleoseismicity of the Cascadia subduction zone: evidence from turbidites off Oregon-Washington Margin: Tectonics, v. 9, p. 569-583.
- Anastasakis, G.C., and Piper, D.J.W., 1991, The character of seismo-turbidites in the S-1 sapropel, Zakynthos and Strofades basins, Greece: Sedimentology, v. 38, p. 717-733.
- Blais-Stevens, A., and Clague, J.J., 2001, Paleoseismic signature in late Holocene sediment cores from Saanich Inlet, British Columbia, Marine Geology, 175, p. 131-148.
- Cifuentes, I.L., 1989, The 1960 Chilean earthquakes. J. Geophys. Research, 94 (B1), 665-680.
- Goldfinger, C., Hans Nelson, C., and Johnson, J.E., 2003, Holocene Earthquake records from the Cascadia Subduction Zone and Northern San Andreas Fault Based on precise dating of offshore turbidites: Annual Reviews of Earth and Planetary Sciences, v. 31, p. 555-577.
- Grantz, A., Phillips, R.L., M.W., M., Starratt, S.W., Jones, G.A., S., N., and Finney, B.P., 1996, Character, paleoenvironment, rate of accumulation, and evidence for seismic triggering of Holocene turbidites, Canada Abyssal Plain, Arctic Ocean: Marine Geology, v. 133.
- Heezen, B.C., and Ewing, M., 1952, Turbidity currents and submarine slumps, and the a929 Grand Banks earthquake: American Journal of Science, v. 250, p. 849-873.
- Inouchi, Y., Kinguasa, Y., Kumon, F., Nakano, S., Ysumatsu, S., and Shiki, T., 1996, Turbidites as records of intense paleoearthquakes in Lake Biwa, Japan: Sedimentary Geology, v. 104, p. 117-125.
- Lomnitz, C., 1970, Major earthquakes and tsunamis in Chile during the period 1535 to 1955. Geologische Rundschau, 59, 938-960.
- Nakajima, T., and Kanai, Y., 2000, Sedimentary features of seismoturbidites triggered by the 1983 and older historical earthquakes in the eastern margin of the Japan Sea: Sedimentary Geology, v. 135, p. 1-19.

6. Dank

Das diesem Bericht zugrundeliegende Vorhaben wurde mit Mitteln des Bundesministeriums für Bildung und Forschung unter dem Förderkennzeichen FV 03G0595A gefördert. Für die geleistete Unterstützung sei hier ausdrücklich gedankt.

BUNDESANSTALT FÜR
GEOWISSENSCHAFTEN UND ROHSTOFFE

16. Dezember 2005

Abteilungsleitung
Geophysik, Meeres-
und Polarforschung

Projektleiter

(Dr. H.-R. Kudrass)
Direktor und Professor

(Dr. M. Wiedicke-Hombach)
Geologiedirektor

Erfolgskontrollbericht

1. Beitrag der Ergebnisse zu den förderpolitischen Zielen des Förderprogramms

Das Vorhaben trägt zu den Zielen bei, die für die aktuellen Themen der „Kontinentränder“ im Rahmen des Sonderprogramms GEOTECHNOLOGIEN des BMBF und der DFG definiert wurden.

Als Teil des Verbundvorhabens TIPTEQ. (from the incoming plate to mega-thrust earthquake processes) sind hier besonders die Steuerfaktoren für Subduktionsbeben und die Prozesse in der seismischen Kopplungszone konvergenter Plattenränder sowie die Entwicklung des Arc-Forearc Systems zu nennen. Als Element des Teilprojekts ‚Koseismische Massenumlagerungen‘ trägt es besonders bei zu dem Ziel, die Rekurrenz holozäner Starkbeben in Chile zu ermitteln, um neue Strategien der Gefährdungs-einschätzung und ggf. eine Überwachung von Starkbeben an konvergenten Platten-rändern entwickeln zu können.

2. Wissenschaftlicher und technischer Erfolg des Vorhabens

Die wissenschaftlichen Erfolge des Projekts sind in den beigefügten Manuskripten zur Publikationen dargelegt. Ferner wurde auf nationalen und internationalen Tagungen darüber berichtet (siehe Liste A1).

3. Finanzierungs- und Zeitplan

Der ursprünglich vorgesehene Finanzierungs- und Zeitplan (Beginn 1.1.2004) wurde um 4 Monate verschoben, da Anfang 2004 zunächst ein Projektmitarbeiter gewonnen werden musste, der dann zum 1. Mai 2004 eingestellt werden konnte.

4. Verwertbarkeit der Ergebnisse und Verwertungsmöglichkeiten

Die erzielten Ergebnisse stellen Beiträge zur Grundlagenforschung dar, auf denen durch Folgeprojekte aufgebaut wird. Eine marktwirtschaftliche Verwertbarkeit ist nicht gegeben.

5. Erfindungen und Schutzrechtsanmeldungen

Erfindungen und Schutzrechtsanmeldungen haben sich durch die Forschungstätigkeiten nicht ergeben, da durchgehend bekannte und gängige Verfahren eingesetzt wurden.

6. Arbeiten, die zu keiner Lösung geführt haben

Entfällt

A - 1

Liste von Vorträgen und Postern

Poster

Reichel, T., Wiedicke, M., Huebsch, C., (2004) Turbiditic Sequences in sediment cores from the continental margin of Southern Chile as a potential record of seismic activity, Poster Presentation, 2004 AGU-Annual Fall Meeting San Francisco, 13-18 December.

Reichel, T. & Wiedicke, M. (2005), Turbiditic Sequences in Sediment Cores from the Continental Margin of Southern Chile as a Potential Record of Seismic Activity, Statusseminar FS SONNE, 9.-11.3.2005, Warnemünde, Tagungsband S.175-177.

sowie

Völker, D., Reichel, T., Heubeck, C., Wiedicke, M. (2003), Turbiditic cover of Southern Chilean seamounts: remnants of “giant uphill” turbidity currents, Sediment conference, October 2003, Chile.

Völker, D., Reichel, T., Heubeck, C., (2003), Turbiditic cover of Southern Chilean seamounts: traces of „giant uphill“ turbidity currents, SEDIMENT 2003, Wilhelmshaven.

Vorträge

Wiedicke, M. & Reichel, T. (2005), Turbiditic Sequences in Sediment Cores from the Continental Margin of Southern Chile as Archive of past Seismic Activity. Statusseminar Kontinentränder, 9.-10. Juni 2005, GFZ Potsdam, Science Report no. 5, p.82-84.

Reichel, T. & Wiedicke, M. (2005), Seismoturbidite – Aktuelle Projektergebnisse. TIPTEQ - Kooperationssitzung, April 2005, GFZ-Potsdam.

Reichel, T. & Wiedicke, M. (2005), Starkbeben und submarine Massenumlagerungen - Seismoturbidite vor Chile (TIPTEQ-Projekt). BGR – Hauskolloquium, März 2005.

A - 2

Publikationen

1

Reichel, T., Wiedicke, M., Schettler, G., Rein, B. (in prep), *Seismoturbidites - a potential record of historic strong earthquakes at the Continental Margin of Chile* (einzureichen bei Marine Geology)

sowie

2

Völker, D., Reichel, T., Heubeck, C., Wiedicke, A. (eingereicht), *Turbiditic cover of Southern Chilean seamounts: traces of „giant uphill“ turbidity currents*, (eingereicht bei Marine Geology), 21 pp.

to be submitted to Marine Geology

Seismoturbidites at the Continental Margin of Chile

T. Reichel¹, M. Wiedicke¹, G. Schettler², B. Rein³

¹ Bundesamt für Geowissenschaften und Rohstoffe
Stilleweg 2, D-30655 Hannover, Germany

² Geoforschungszentrum Potsdam
Telegrafenberg, D-14473 Potsdam Germany

³ Institut für Geowissenschaften, Johannes Gutenberg Universität Mainz,
Becherweg 21, D-55128 Mainz, Germany

Table of content:

Abstract:.....	1
1. Introduction	2
2. Working Area and Setting.....	2
2.1 Tectonic setting	2
3. Material and Methods.....	4
3.1. Spectrolino	4
3.2 X-ray Photographs	4
3.3 Magnetic susceptibility and Gamma ray attenuatuion	5
3.4. AMS ¹⁴ C - Analysis	5
3.5. ²¹⁰ Pb analysis	5
4. Results and data interpretation	6
4.1. X-ray photographs, Spectrolino, Magnetic susceptibility and Gamma Counts	6
4.2 Radiometric results - AMS ¹⁴ C and ²¹⁰ Pb.....	6
5. Discussion of results.....	7
6. References	9
7. Figures:.....	12

Abstract:

During RV SONNE cruise SO-161 a 5.7 m long sediment core was obtained from a slope basin at the continental margin of Chile. The sequence contains 9 major turbidite beds. The layers are up to 70 cm thick, commonly show erosive contacts to the underlying sediments and according to their internal sediment textures are proximal turbidite deposits. Hemipelagic sediments in relatively thin intervals between the turbidite deposits were identified in X-ray photos and by colour reflectance measurements. Samples from the hemipelagic sections were used for AMS¹⁴C age determination and at the core top for ²¹⁰Pb analysis. According to the derived age model the second turbidite bed above the core base was deposited before 1279 AD (age: 726a BP) and the turbidite layer above before 1403 AD (602a BP). The remaining 6 turbidite deposits can – despite some uncertainties - be correlated with major earthquakes in southern Chile as known from the historical record.

Keywords: seismoturbidite, earthquake, recurrence rate, continental margin, Chile, AMS ¹⁴C, lead-210

1. Introduction

The relationship between seismic events and mass-wasting processes has long been observed. An excellent example for this relationship has been presented by Heezen & Ewing (1952) at the Atlantic continental margin of Canada: the strong 1929 Grand Bank earthquake triggered a huge turbidity flow, the velocity and spreading of which could be precisely determined due to successively rupturing of deep-sea telephone cables in the vicinity of the mass-flow event. However, there is more than one mechanism which can trigger mass-wasting processes, e.g. storm waves, river floods, earthquakes, tsunamis etc.. Adams (1990) presented a compilation of such processes based on sediment analyses of cores from the continental margin of Oregon. Recently, some authors attempted to determine characteristics of seismically derived turbidite deposits, these included the extent of the area affected, the relatively large volume of remobilised sediment (Gorsline et al., 2000), and reverse gradation (Nakajima and Kanai, 2000). Other investigations concentrated on lake deposits where successful correlations to earthquakes have been achieved (Inouchi et al., 1996; Shiki et al. 2000; Schnellmann et al., 2002); or studies in marginal seas (Anastasakis & Piper, 1991) or at continental margins (Goldfinger et al. 2003; Grantz et al., 1996, Karlin & Abella, 1992; Nelson et al., 1995).

Precise age-dating of sediments, large extent of turbidite beds of more than one source area, and the calibration with known historic seismic events appear to be the most promising approach for defining ‘seismo-turbidites’. In this study we apply this approach to core material from the Chilean continental margin.

2. Working Area and Setting

2.1 Tectonic setting

The active margin of Chile is characterized by subduction of the oceanic Naszca-Plate beneath the South American plate. Since at least 48 Ma oceanic crust has been subducted below the South American Continent along the Peru and Chile coasts. The subduction occurs slightly oblique and is directed towards the NE (Cembrano et al., 2000).

The convergence of crustal plates generates ongoing tectonic activity. In 1960, Chile was the location of the magnitude 9.5 earthquake – the strongest seismic event registered so far. Its rupture length was estimated to more than 1000 km based on crustal deformation and the distribution of aftershocks (starting at 37°S and extending 1000 km southwards, Cifuentes, 1989). An overview of the frequent seismic event is presented by Lomnitz (1970).

Currently, the relevant section of the subsiding oceanic Nazca plate is characterized by 2 inactive major fault zones which are characterized by chains of seamounts running slightly oblique relative to the direction of subduction: the Mocha fault zone between 38 and 39°S and the Valdivia fault zone at approximately 40°S (**Fig. 1**). Onshore, at the continental plate of South America, three major fault zones define the setting in the working area between 37° and 39°S: (1) the N-S striking Liquiñe-Ofqui-Fault zone (LOFZ), which runs parallel to the axis of the depression within the magmatic arc, (2) the NW-SE striking Bio-Bio-Fault Zone in the North of our working area and (3) the Gastre-Fault Zone further south (Cembrano et al., 2000; Herve, 1994). Seismically the continental margin can be divided into a sequence of sections following in N-S direction; at 37-38°S a relatively short transition zone can be recognised which appears to be particularly active (Nishenko, 1985).

2.2 Working Area

Our working area is located at the continental slope of southern Chile between 36°S and 40°S. Cores were taken at the slope and the neighbouring deep sea trench. The foot of the slope marks the deformation front which is the boundary between the two above mentioned crustal plates (**Fig. 1**). The slope is composed of a relatively narrow shelf area followed by a topographically irregular margin with small ridges, slope basins and deeply incised canyons off the major river mouths. Slope inclination generally ranges between 2.5° and 4.0°. Towards the lower margin the slope tends to become steeper with angles often exceeding 10° (**Fig. 2**). Most of the intra-slope basins occur at the lower part of the margin which often is composed of accretionary sequences which experience significant tectonic faulting and selective uplift over time. Accordingly these basins commonly show an infill of well stratified sediments as can be demonstrated in seismic profiles and sediment echosounder data. The deep sea trench following seawards of the lower slope is 60-80 km wide, and accumulated a 2-3 km thick sediment fill composed of turbiditic sequences and fan deposits (Bangs and Cande, 1997; Reichert and shipboard party, 2002). The trench surface is slightly inclined to the North and exposes an axial channel which is several km wide and about 200 m deep. It can be followed for several hundred kilometres along the trench. The rough topography of the Naszca plate which is covered by a thin pelagic sediment veneer only, forms the seaward boundary of the trench.

Core SL 112 of this study was taken during SONNE cruise SO161-5 from an intraslope basin located in 4130 m water depth close to the foot of the continental margin. This basin receives sediment influx from a particularly large slope area of more than 170 km² (**Fig. 3**) Sediment echosounder profiles of the basin fill show well stratified sediments – a seismic facies typical for turbiditic sequences. Slope basins like the one sampled are excellent receptacles for

mass flow processes resulting from episodic destabilizations of sediment at the continental margin

3. Material and Methods

For the retrieval of sediment cores a 10 m long gravity corer with a 2.5 tons heavy led weight was deployed. Coring position SL112 is located at 38° 04.84'S and 74°29.80'W in 4130 m water depth. Recovered core length is 5.7 m. Immediately after retrieval the core was logged in 1 cm intervals using a multi sensor core logger (MSCL) from GEOTEK: gamma-ray attenuation, p-wave velocity and magnetic susceptibility were measured. The core was then split open and the sediments were described lithologically. For further investigations the core was sealed and stored at 4°C.

3.1. Spectrolino

The sediment core was scanned with a Colour scanner ‘Spectrolino’ (from GretagMcBeth) in consecutive 5 mm intervals. The device measures calibrated reflectance spectra between 380 nm and 730 nm wavelength. The reflectance spectra include several absorption bands which are related to plant pigments involved in photosynthesis. Of particular interest is an absorption band minimum at 660-670 nm which is considered indicative for absorption by the pigment chlorin (Rein, 2003; Rein et al., subm.; Rein and Sirocko, 2002, 2003).

The ratio of reflectance between 570 (R570) and 630 (R630) nm wavelength monitors a characteristic change of the reflectance spectrum continuum. A shift of maximum reflectance is correlated to a change of the coarse grained fraction or the amount of rock debris. It is used to identify / verify turbiditic layers (Rein, 2003; Rein et al., subm.; Rein et al., 2004; Rein & Sirocko, 2002, 2003).

3.2 X-ray Photographs

X-ray radiographs were taken of 1 cm thick sediment slices sealed in plastic boxes of 20 cm length and 10 cm width. A Philips 80KV energy source was used, mounted at a distance of 1.2 m above the sample; the radiographs were fabricated of Agfa D4 Structurix film using an exposure time of 30 sec. The film negatives were scanned in high resolution with a standard PC scanner and then colour inverted with a standard graphic program. The resulting X-ray photographs reveal high-resolution images of internal sediment structures. Light-coloured sections of the photographs are related to sediment layers with high density and/or coarse sediment components, whereas gray and dark sections depict homogenous hemipelagic mud (**Fig. 4**).

3.3 Magnetic susceptibility and Gamma ray attenuatuion

The average susceptibility value of the core is 2.6×10^3 SI; hemipelagic sediments display slightly lower values of about 2.2×10^3 SI, whereas turbiditic layers show values of up to 4×10^3 SI. Susceptibility profiles across a turbidite layer nicely depict the graded character of the sediment layer with the highest values at the base and a decrease towards the top of the layer (**Fig. 5**).

The gamma-ray attenuation is related to the density of the sediment. For the purpose of this study the uncalibrated curve (counts per second) is used to monitor relative changes in sediment density and thus easily identify / verify turbidite layers.

Both parameters - magnetic susceptibility and density profiles - were used as tools to improve the characterisation of turbidite layers.

3.4. AMS ^{14}C - Analysis

After turbidites were identified using the above described methods sediment samples were taken for AMS ^{14}C analysis. Sediment samples were freeze dried and then wet-sieved (63 μm); 5-10 mg of tests of planktonic foraminifera were picked for analysis. The AMS ^{14}C analyses were carried out at the Leibniz laboratory in Kiel. Radiometric AMS ^{14}C ages were calibrated with the software Calib 4.4 (McCormac et al., 2002; Stuiver et al., 1998a; Stuiver et al., 1998b). As the sample location is relatively close to the East Pacific upwelling zone, a reservoir age of 580 years was used for the calculation of the calendar age following Shackleton et al. (1988).

Samples were taken below each turbidite base to define the age of deposition immediately prior to the 'event'. In several sampling depths we did not succed to extract enough calcitic tests to conduct an analysis. The lack of calcitic tests is partly due to the water depth of core SL 112 of 4130 m which is below the calcite compensation depth (Lisitzin, 1996; McCarthy, 2004).

3.5. ^{210}Pb analysis

15 sediment samples form the uppermost 23 cm of core SL112 were analysed by gamma spectrometry for lead-210 activity. Total activity of ^{210}Pb ($^{210}\text{Pb}^{\text{total}}$) was determined by α -spectrometric measurement of ^{210}Po (Equipment: 8-chamber Alpha-Analyst, Canberra; procedure described by Flynn [1968]). Unsupported lead-210 ($^{210}\text{Pb}^{\text{exc}}$) is calculated from the difference between $^{210}\text{Pb}^{\text{total}}$ and $^{210}\text{Pb}^{\text{supp}}$. **Figure 6** shows the activity curve of $^{210}\text{Pb}^{\text{exc}}$ versus depth for the upper core section of core SL112.

4. Results and data interpretation

4.1. X-ray photographs, Spectrolino, Magnetic susceptibility and Gamma Counts

Turbiditic sequences are characterized by brighter colours in the x-ray photographs as they contain a higher amount of coarser material with higher density than the surrounding background sediments of hemipelagic origin. Details of the textures identified in the x-ray images allow to distinguish between particular Bouma units (commonly Tb to Te) which are characteristic of turbidite deposits (Bouma, 1962).

The magnetic susceptibility is also distinctly enhanced in those sediment sections of core SL112 which were identified as turbidite layers based on x-ray images (**Figs. 4 & 5**). The average level of the magnetic susceptibility of the core is 2.6×10^3 SI, while that of the hemipelagic sediments is slightly lower (2.2×10^3 SI); turbiditic layers show values of up to 4×10^3 SI (**Fig. 6**) which can be explained by more abundant and coarser grained magnetic particles of volcanic origin. Accordingly, the base layer of each turbidite bed displays the highest susceptibility values which then decrease towards the top of the layer, thus nicely mimicking the graded grain-size character of the bed.

The density profiles show a continuous increase (that is a decrease of cps) towards the core base which indicates the successive compaction of terrigenous sediments with time. The hemipelagic sediment sections display the lowest densities (higher count rate). The gamma-ray attenuation data also exhibit the graded character of the turbidite layers with densities decreasing towards the top of the bed (**Figs 5 & 6**). These characteristics have been used to verify our initial lithological interpretation of the core. The colour scanning data support these results. Sediment sections with a high fraction of rock debris and coarse clastics (e.g. turbidite beds) are characterized by maxima of the 570 nm vs. 630 nm wavelengths ratio. The highest ratio is commonly associated with the base layer of turbidites in core SL 112.

Combining all these indications of turbidite layers in the sequence of core SL 112 results in the definition of 9 fairly thick main turbidite beds (**Fig. 5**).

4.2 Radiometric results - AMS¹⁴C and ²¹⁰Pb

AMS¹⁴C

Two samples contained sufficient carbonate shells to provide a reliable radiocarbon date: sample SL112-470cm and sample SL112-535cm. After calibrating the radiocarbon ages the first sample was determined to be 602 a BP (range: 555-565, and 597-631). The second and deeper sample is slightly older and has an age of 726 a BP (range: 684-704 and 718-744). As both of the samples were taken below the base of a turbidite bed, they approximately

determine the time interval between these two sedimentation events: it amounts to 124 years.

^{210}Pb

Figure 6 shows the depth plot of unsupported lead-210 ($^{210}\text{Pb}^{\text{exc}}$). At 20.5 cm the activity of $^{210}\text{Pb}^{\text{exc}}$ is close to the detection limit of $^{210}\text{Pb}^{\text{exc}}$. The $^{210}\text{Pb}^{\text{exc}}$ of the sediment section above the uppermost turbidite exponentially declines close to the rather constant $^{210}\text{Pb}^{\text{exc}}$ value obtained in the upper part of the turbidite. Hemipelagic sediments below the turbidite show a higher $^{210}\text{Pb}^{\text{exc}}$ activity than the sample immediately above the turbidite. In the semi-logarithmic plot ($^{210}\text{Pb}^{\text{exc}}$ vs. depth) samples from above and below the turbidite clearly define separate linear trend lines.

The mean sediment rates [SR(mm/yr)] based on $^{210}\text{Pb}^{\text{exc}}$ analyses are given by: SR = $\lambda 210\text{Pb} \cdot 10 / \text{grad}$ (grad= gradient of the trend lines) using the CIC-model approach (Constant Initial Concentration). According to these calculations sediments above the turbidite were deposited at a mean sedimentation rate of 0.4173 mm/yr. Assumed porosity of 0.9 and a density value of 2.3 g/cm³ for the solid sediment gives mean annual mass accumulation of 96 g m⁻² yr⁻¹ for most recent hemipelagic sedimentation. The calculated initial $^{210}\text{Pb}^{\text{exc}}$ of the topmost sample is 0.876 Bq/g which corresponds to a $^{210}\text{Pb}^{\text{exc}}$ -flux of 84.1 Bq m⁻² yr⁻¹. We did not find monitoring data for the atmospheric flux of $^{210}\text{Pb}^{\text{exc}}$ for the studied site in the open literature. It is therefore unclear if $^{210}\text{Pb}^{\text{exc}}$ -flux values in the order of 80 Bq m⁻² yr⁻¹ or even above may originate from atmospheric deposition at the core location alone.

For the purpose of this study we use the steep decline of the $^{210}\text{Pb}^{\text{exc}}$ curve and the presence down to a core depth of 20.5 cm as an indication that the core basically covers the entire time interval from the present to about 700 years BP.

5. Discussion of results

According to our radiometric age model ($^{210}\text{Pb}^{\text{exc}}$) the upper turbidite dates around AD 1900. This age determination would make the turbidite bed too old to correlate with the 1960 seismic event. However, due to the extremely sensitive depth scale (with few millimeters changing the age by tens of years), we are not sure, whether we over-interpret the data. A ^{137}Cs peak due to enhanced influx from atmospheric nuclear tests is expected at 1.6 cm depth but couldn't be verified. Either the most recent sediment layers got lost during the coring procedure, or the local ^{137}Cs activities at that deep water site are below the detection limit.

In any way the steep decline of the $^{210}\text{Pb}^{\text{exc}}$ curve and the presence of unsupported ^{210}Pb isotopes down to 20.5 cm suggests that only few centimetres of the soft surface layer may be missing. Thus the core basically represents sediments from the entire time interval of the past 700 years.

Within this sediment sequence 9 major sedimentation events have been determined based on x-ray images and logging and colour scanning results. For a correlation of our core sequence with paleoseismic events we used the data of major historical earthquakes from literature data as described and analysed by Lomnitz (1970) and Cifuentes (1989). A question arises how to properly define the number of events that effect a given location. As has been demonstrated e.g. by the recent Sumatra event, mega earthquakes may affect areas of more than a thousand kilometres length. Thus, knowledge of the geographical extent of the effects of strong earthquakes is crucial, which for past events hasn't always been properly determined or is difficult to be defined e.g. for sparsely populated areas. Structurally, a segmentation of the active margin in Chile can be observed with an associated characteristic distribution for strong seismic events. Nishenko (1985) distinguished three geographic segments – from latitude 35°S to 37°S, then from 37°S to 39°S and from 38°S to 46°S. The recurrence rates for the three segments are (from N to S): 92+15 a, 13+10 a and 128+62 a respectively. These figures should be taken as an orientation only as they do not necessarily consider the extent of affected areas of individual seismic events. Cifuentes took a somewhat more general approach assessing the recurrence rate for strong seismic events in central-southern Chile to be 150 a. Thus, when comparing the list of historical earthquakes with our sequence of sedimentation events of core SL112 caution should be exercised.

Figure 7 presents such a correlation effort. The epicentres of the seismic events selected for comparison are scattered geographically between Valdivia in the south and Concepción in the north (distance: ~330 km) with our core position located in between. 8 historical earthquakes fall into the time interval of the past 600 years which is the timespan represented in the topmost dated core section of 4.5 m length. 6 major turbidite beds correspond to the 8 seismic events. Still we think that a valid correlation can be obtained if the extremely short timespan is considered between some of the seismic events. We suggest, that the timespan of 2 years, resp. 5 years between two events (e.g. 1570/1575 and 1835/1837) is too short to ensure a separate imprint in the sedimentary record. The time may be too short to accumulate significant amounts of sediment that can be remobilised by the subsequent seismic event and then deposited as turbidite bed.

Another point of discussion arises from the ^{210}Pb analyses. If the calculated sedimentation rates are strictly applied, the upper turbidite bed is too old to correspond to the 1960 seismic event. As a few centimetres of sediment may be missing (due to the coring process) the exact age of the bed cannot be determined properly. This suggests that the 1960 turbidite

bed is within the missing sediment layers. Despite these uncertainties we consider our correlation effort in principle as valid. This is supported by the time interval of 124 years, which we determined as the increment between two major turbidites in core SL112. This time interval is in the same order of magnitude as the seismic recurrence rate for strong earthquakes (Cifuentes, 1989; Nishenko, 1985). For a more detailed interpretation of the sedimentary sequence more cores need to be analysed for an across-basin correlation of events. Much depends on accurate age determination, which remains a challenge at the deep seated sites of the Chilean margin.

6. References

- Adams, J., 1990, Paleoseismicity of the Cascadia subduction zone: evidence from turbidites off Oregon-Washington Margin: *Tectonics*, v. 9, p. 569-583.
- Anastasakis, G.C., and Piper, D.J.W., 1991, The character of seismo-turbidites in the S-1 sapropel, Zakynthos and Strofades basins, Greece: *Sedimentology*, v. 38, p. 717-733.
- Bangs, N.C., and Cande, S.C., 1997, Episodic development of a convergent margin inferred from structures and processes along the southern Chile margin: *Tectonics*, v. 16, p. 489-503.
- Bouma, A.H., 1962, *Sedimentology of some Flysch Deposits: A Graphic Approach to Facies Interpretation*: Amsterdam, Elsevier, 168 p.
- Cembrano, J., Schermer, E., Lavenu, A., and Sanhueza, A., 2000, Contrasting nature of deformation along an intra-arc shear zone, the Liquie-Ofqui fault zone, Southern Chilean Andes: *Tectonophysics*, v. 319, p. 129-149.
- Cifuentes, I.L., 1989, The 1960 Chilean earthquakes. *J. Geophys. Research*, 94 (B1), 665-680.
- Clayton, T., and Kemp, A.E.S., 1990, Clay mineralogy of Cenozoic sediments from the Peruvian continental margin: Leg 112, in Suess, E., von Huene, R., and participants, a., eds., *Proceedings of the Ocean Drilling Program*, p. 59-86.
- Goldfinger, C., Hans Nelson, C., and Johnson, J.E., 2003, Holocene Earthquake records from the Cascadia Subduction Zone and Northern San Andreas Fault Based on precise dating of offshore turbidites: *Annual Reviews of Earth and Planetary Sciences*, v. 31, p. 555-577.
- Gorsline, D.S., DeDiego, T., Nava-Sanchez, E.H., 2000., Seismically triggered turbidites in small margin basins: Alfonso Basin, western Gulf of California and Santa Monica Basin, California Borderland, *Sedimentary Geology*, 135, p. 21-35.
- Grantz, A., Phillips, R.L., M.W., M., Starratt, S.W., Jones, G.A., S., N., and Finney, B.P., 1996, Character, paleoenvironment, rate of accumulation, and evidence for seismic triggering of Holocene turbidites, Canada Abyssal Plain, Arctic Ocean: *Marine Geology*, v. 133.

- Heezen, B.C., and Ewing, M., 1952, Turbidity currents and submarine slumps, and the a929 Grand Banks earthquake: American Journal of Science, v. 250, p. 849-873.
- Herve, F., 1994, The Southern Andes between 39° and 44°S latitude: the geological signature of a transpressive tectonic regime related to a magmatic arc, *in* Reutter, K.-J., Scheuber, E., and Wigger, P., eds., Tectonics of the Southern Central Andes: Berlin, Springer-Verlag, p. 243-248.
- Inouchi, Y., Kinguasa, Y., Kumon, F., Nakano, S., Ysumatsu, S., and Shiki, T., 1996, Turbidites as records of intense paleoearthquakes in Lake Biwa, Japan: Sedimentary Geology, v. 104, p. 117-125.
- Karlin, R.C., and Abella, S.E.B., 1992, Paleoearthquakes in the Puget Sound region recorded in sediments from Lake Washington: Science, v. 258, p. 1617-1620.
- Lisitzin, A.P., 1996, Oceanic Sedimentation: Lithology and Geochemistry, American Geophysical Union, 400 p.
- Lomnitz, C., 1970, Major Earthquakes and Tsunamis in Chile during the period 1535 to 1955: Geologische Rundschau, v. 59, p. 938-960.
- McCarthy, F.M.G., 2004, The micropaleontological character of anomalous clacerous sediments of late Pliocene through early Pleistocene age below the CCD in the northwestern North Pacific Ocean: Palaeogeography, Palaeoclimatology, Palaeoecology, v. 215, p. 1-15.
- McCormac, F.G., Reimer, P.J., Hogg, A.G., Higham, T.F.G., Baillie, M.G.L., Palmer, J., and Stuiver, M., 2002, Calibration of the Radiocarbon Time Scale for the Southern Hemisphere: AD 1850-950: Radiocarbon, v. 44, p. 641-651.
- Nakajima, T., and Kanai, Y., 2000, Sedimentary features of seismoturbidites triggered by the 1983 and older historical earthquakes in the eastern margin of the Japan Sea: Sedimentary Geology, v. 135, p. 1-19.
- Nelson, A.R., Atwater, B.F., Borbowski, P.T., L.A., B., Clague, J.J., Carver, G.A., Darienzo, M.E., Grant, W.C., Krueger, H.W., Sparks, R., Stafford, T.W., and Stuiver, M., 1995a, Radiocarbon evidence for extensive plate-boundary rupture about 300 years ago at the Cascadia subduction zone, v. 378, p. 371-374.
- Nishenko, S.P., 1985, Seismic potential for large and great interplate earthquakes along the Chilean and southern Peruvian margins of South America: A quantitative reappraisal: Journal of Geophysical Research, v. 90, p. 3589-3615.
- Reichert, C., and Party, S.S.S., 2002, Subduction processes off Chile: preliminary geophysical results of SONNE cruise SO-161(2+3), European Geophysical Society, XXVII General Assembly,: Nice, France.
- Rein, B., 2003, In-situ Reflektionsspektroskopie und digitale Bildanalyse Gewinnung hochauflösender Paläoumweltdaten mit fernerkundlichen Methoden [Habilitationsschrift thesis]: Mainz, Johannes Gutenberg-Universität Mainz.

Rein, B., Lückge, A., Reinhardt, L., and Dullo, C.-W., subm., El Niño variability off Peru during the last 20,000 years: Paleoceanography.

Rein, B., Lückge, A., and Sirocko, F., 2004, A major Holocene ENSO anomaly during the Medieval period: Geophysical Research Letters, v. 31, p. L17211, doi:10.1029/2004GL020161.

Rein, B., and Sirocko, F., 2002, In-situ reflectance spectroscopy - analysing techniques for high resolution pigment logging in sediment cores: International Journal of Earth Sciences, v. 91, p. 950-954.

—, 2003, In-situ reflectance spectroscopy - analysing techniques for high resolution pigment logging in sediment cores-Erratum: International Journal of Earth Sciences, v. 92, p. 143.

Schnellmann, M.N., Anselmetti, F.S., Giardini, D., and Ward, S.N., 2002, Prehistoric earthquake history revealed by lacustrine slump deposits: Geology, v. 30, p. 1131-1134.

Shackleton, N.J., Duplessy, J.C., Arnold, M., Maurice, P., Hall, M.A., and Cartlidge, J., 1988, Radiocarbon age of last glacial Pacific deep water: Nature, v. 335, p. 708-711.

Shiki, T., Kumon, F., Inouchi, Y., Kontani, Y., Sakamoto, T., Tateishi, M., Matsubara, H., and Fukuyama, K., 2000, Sedimentary features of the seismo-turbidites, Lake Biwa, Japan: Sedimentary Geology, v. 135, p. 37-50.

Stuiver, M., P.J., R., Bard, E., Beck, J.W., Burr, G.S., Hughen, K.A., Kromer, B., McCormac, G., van der Plicht, J., and Spurk, M., 1998a, INTCAL98 Radiocarbon Age Calibration, 24.000-0 cal BP: Radiocarbon, v. 40, p. 1041-1083.

Stuiver, M., P.J., R., and Braziunias, T.F., 1998b, High precision radiocarbon age calibration for terrestrial and marine samples: Radiocarbon, v. 40, p. 1127-1151 (revised dataset).

7. Figures:

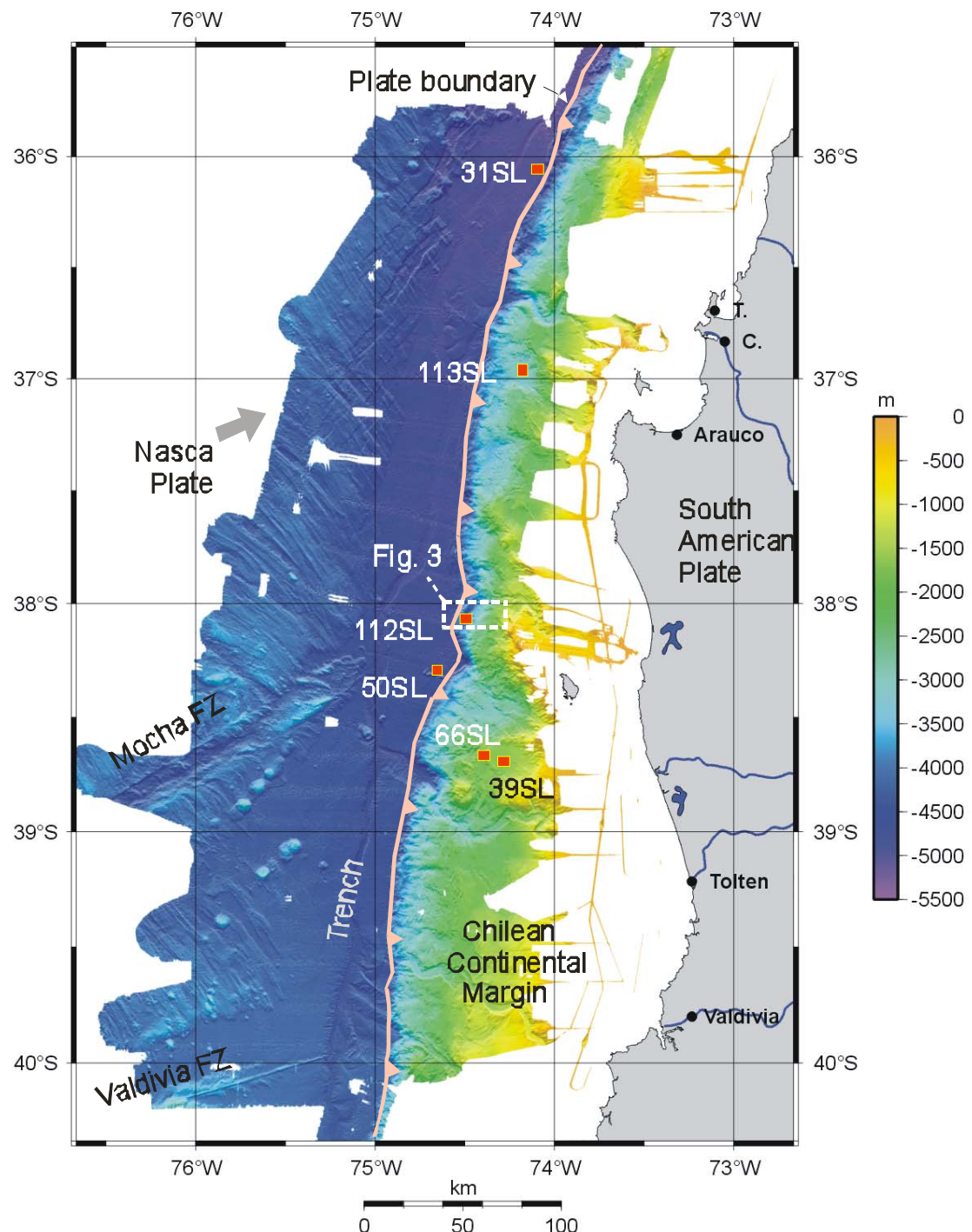


Figure 1: Bathymetric map of the southern Chilean continental margin with the relevant structural features of this segment of the margin. Also shown are positions of cores taken during SO161-5. Core SL112 of this study is located in a basin close to the foot of slope.

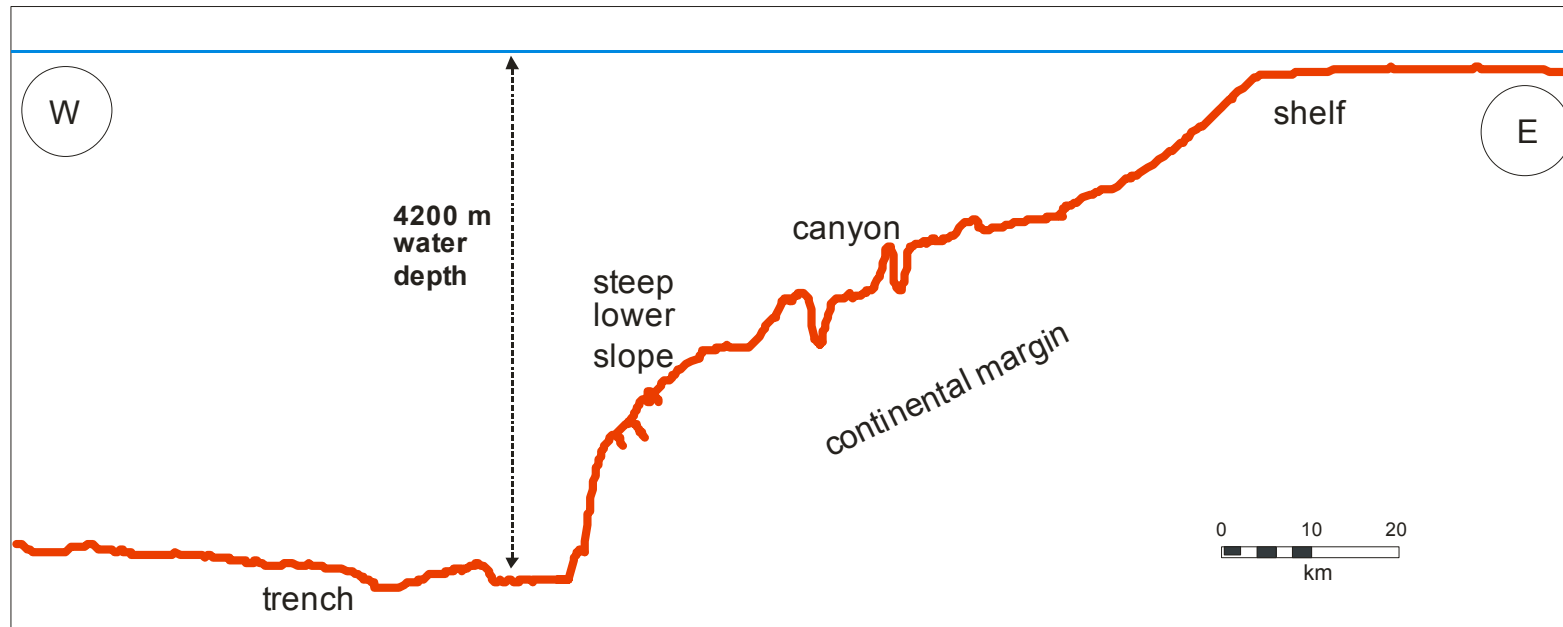


Figure 2: Depth profile across the Chilean continental margin at $38^{\circ}30'S$. Note relatively steep inclination of lower slope section (profile vertically exaggerated).

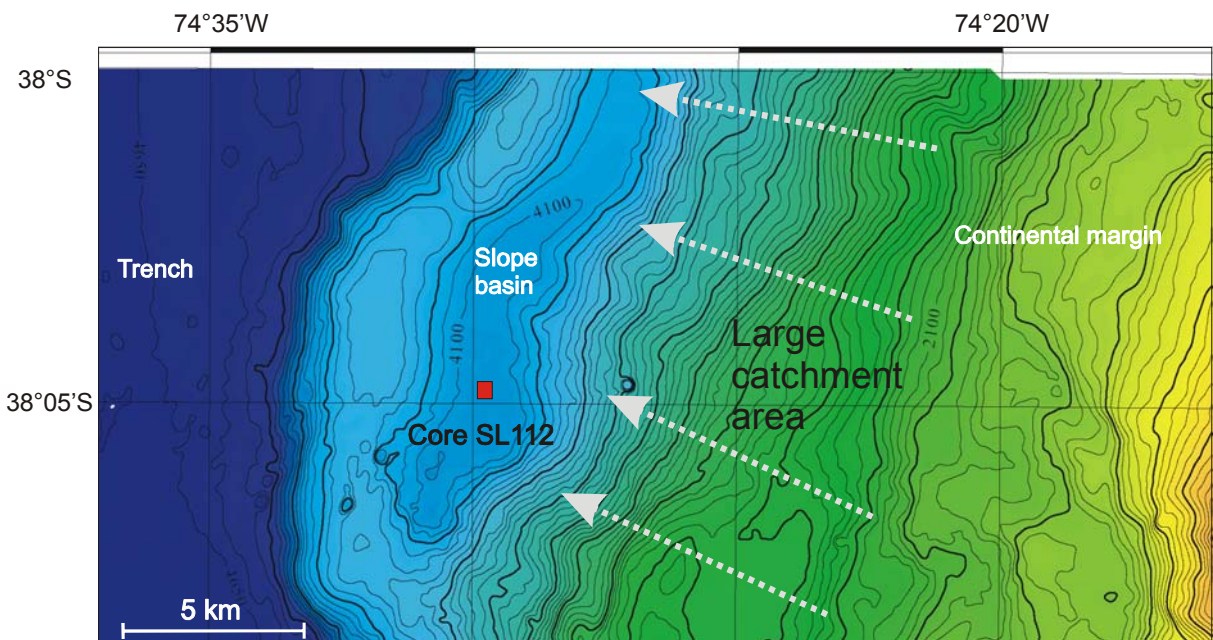


Figure 3: Bathymetric map of slope basin at the foot of the continental margin. The basin exhibits a particularly large catchment area with extended areas of steeply inclined slope. A topographic barrier of 2-300 m elevation separates the basin from the deep sea trench (50 m contour lines).

Figure 4

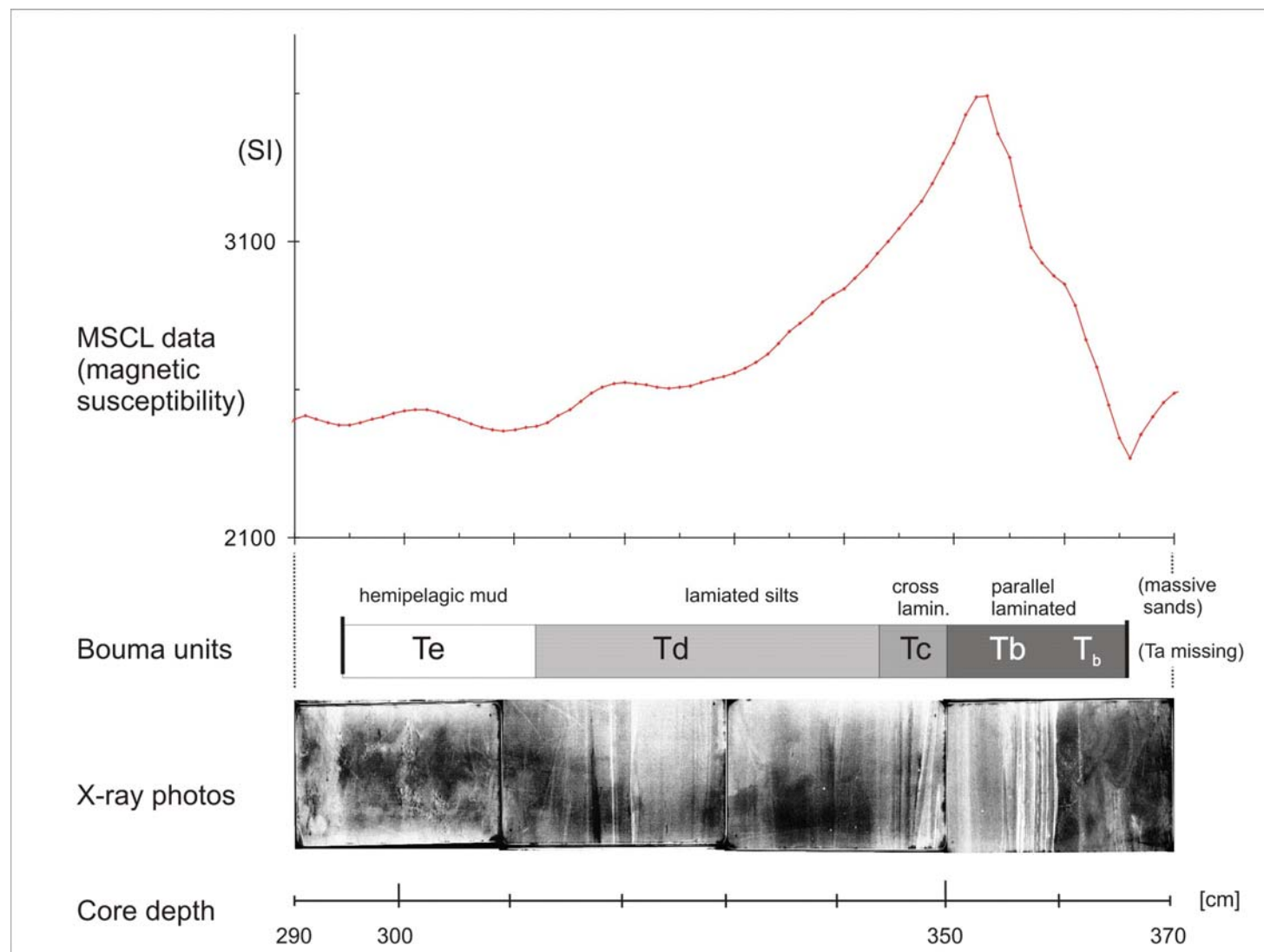


Figure 4: Details of core section 290 - 370 cm of Core SI112. X-ray photos combined with core description and log data allow to distinguish different Bouma subunits within turbidite bed no. 4 (from top; see Fig. 5).

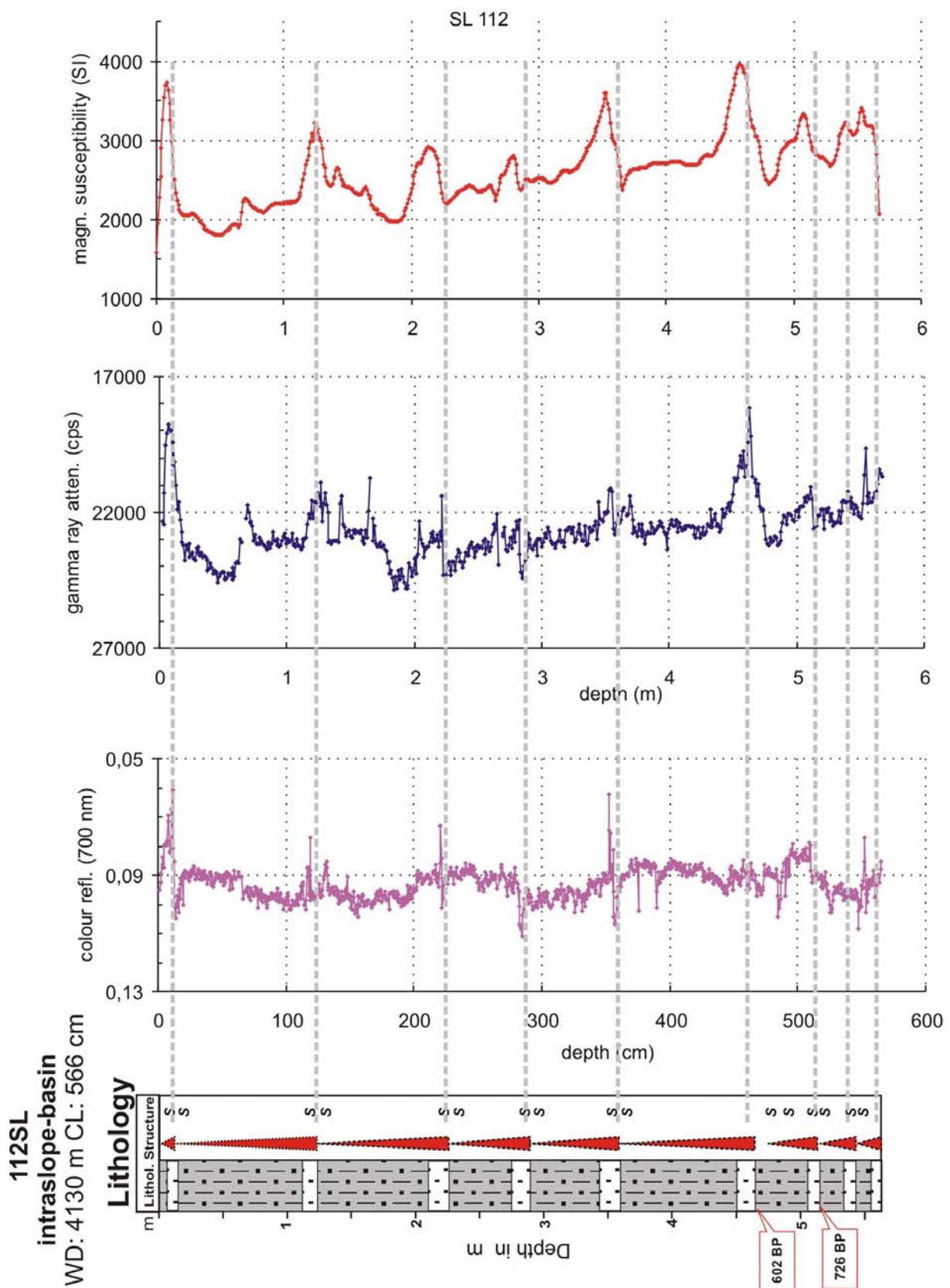


Figure 5: Lithology of core SL112 and its correlation with logging data and colour measurements; note that nine major events can be determined by combining parameters. AMS¹⁴C dating gives two absolute age point of 602 years BP at 4.7 m and 726 years BP at 5.35 m depth.

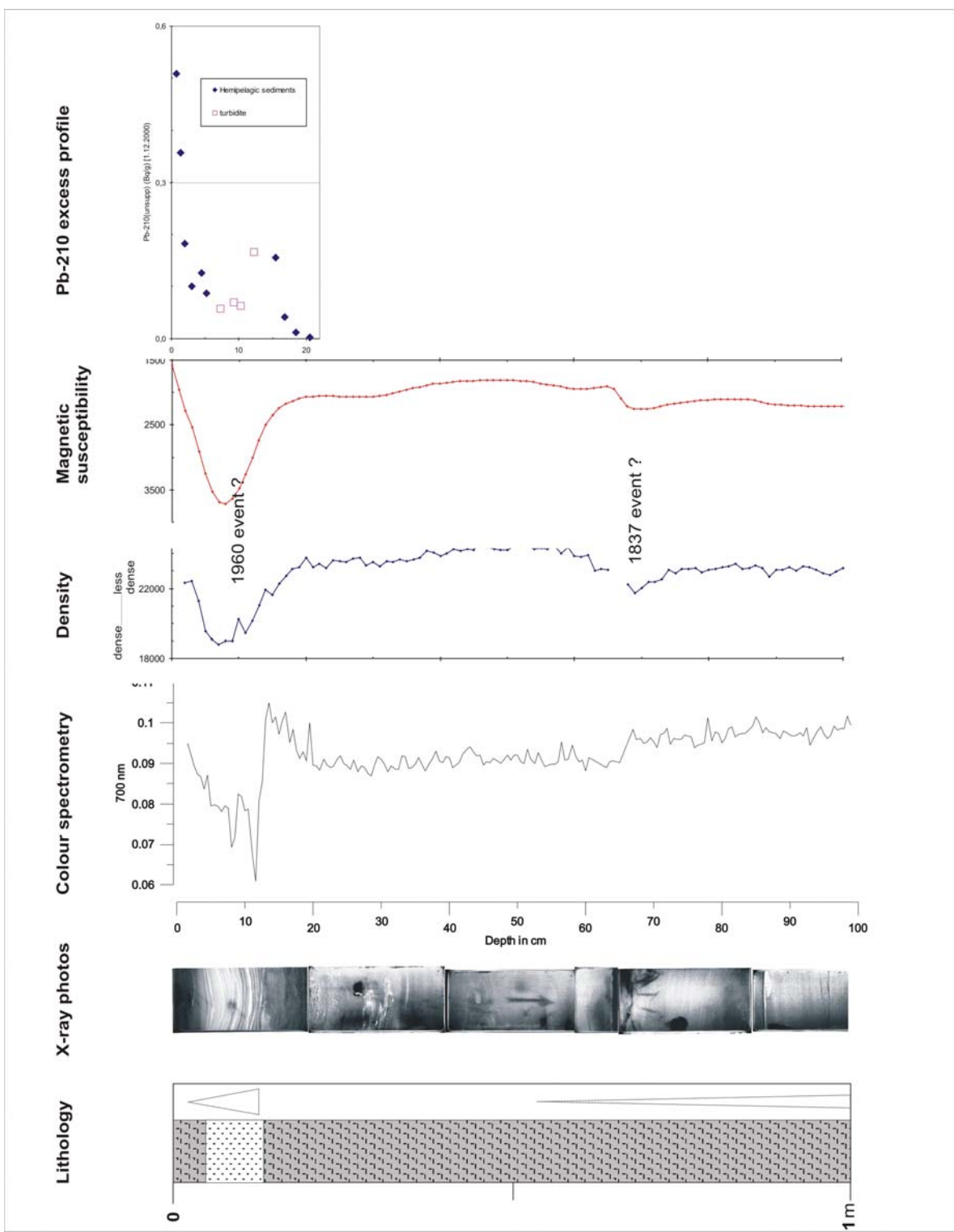


Figure 6: Detailed view of the topmost meter section of SL112, showing the uppermost turbidite layer between 4.5 cm and 13 cm and its expression in the colour profile, density profile (based on gamma ray attenuation and magnetic susceptibility curve). Analysis of ^{210}Pb isotopes proof the presence of $^{210}\text{Pb}_{\text{excess}}$ down to core depth of 20.5 cm. This indicates an age of approximately <150 years at 21 cm depth, supporting a young age of the uppermost significant turbidite bed.

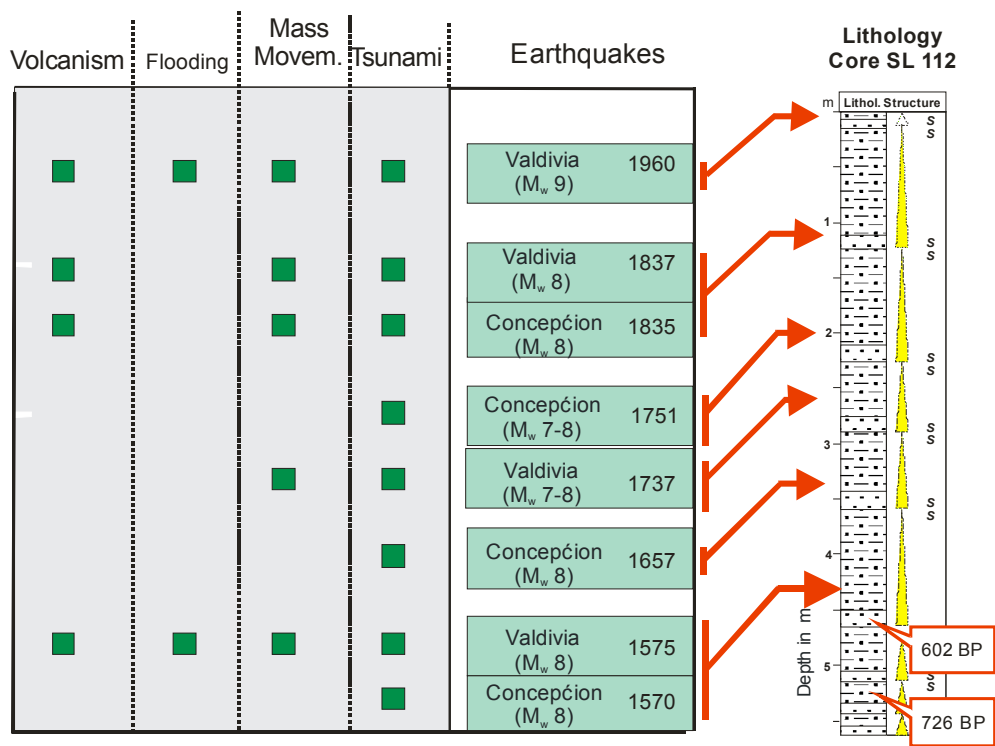


Figure 7: Seismic mega events in southern Chile of the past 450 years and their correlation with the sediment sequence of core SL112.

Submitted to "MARINE GEOLOGY"

Turbiditic cover of Southern Chilean seamounts: traces of “giant uphill” turbidity currents

D. VÖLKER, T. REICHEL, M. WIEDICKE-HOMBACH & C. HEUBECK

During RV SONNE Expedition SO161-5 three gravity cores were obtained on isolated seamounts located within the sediment-filled Peru-Chile Trench off southern Chile. Within these 3.2 m - 7.3 m long cores, numerous turbidite layers were identified. The graded layers are up to 12 cm thick, show sharp contacts to the underlying sediment and are much coarser than the intervals attributed to hemipelagic background sedimentation. Analysis of mineral composition and faunal assemblage of foraminifera within turbidite layers identified particles from upper shelfal to abyssal depths. Oxygen isotope stratigraphy indicates that most of the turbiditic sequence was deposited during the last Glacial and deposition ceased during the Holocene. The topographic setting of our sampling sites, the thickness of several turbiditic layers as well as their maximum grain size indicate suggest that these deposits originated from relatively strong turbide events. Sediment echosounder studies support the existence of widespread turbidite deposition in regions elevated in respect to the floor of the Peru-Chile Trench. The data open the stage for the discussion whether these turbidites are suspension fallout products or bedload deposits from sheet-like turbidity currents overwhelming elevated structures.

Regional setting: geology and oceanography

Bathymetry

The continental margin of Southern Chile between 37°S and 39°S is characterized by a shelf of intermediate width (20-30 km). The shelf edge lies at a water depth of 250 m. The inclination of the continental margin in general ranges between 2.5° and 4.0°. Where small plateaus and slope basins are encountered, the margin displays a stepwise topography with slope angles as steep as 10° (Fig. 2). The continental margin is dissected by three major and some minor deeply incised meandering submarine canyons which have developed off the mouth of large river systems (Biobio, Tolten and Callecalle Canyons). Some of the canyons begin directly at the mouths of the corresponding rivers (e.g. Biobio) and cut into the shelf. The canyons effectively funnel much of the longshore transported sediment as well as fluvial input downslope. Some of the submarine canyons (namely the Biobio Canyon) form a pronounced submarine fan where they enter the trench (Thornburg and Kulm, 1990). Off Southern Chile, the Peru-Chile Trench is filled by up to 2-3 km of predominantly turbiditic sediment (Bangs and Cande, 1997; Reichert, 2002). Due to this infill, the trench does not appear as a bathymetric depression, but rather as a flat abyssal plain of 40 to 60 km width, adjacent to the lowermost slope. The surface of the trench fill is inclined to the North with a slope angle of 0.12°. The trench displays a several km wide and about 150 m deep, slightly winding axial channel. This channel is continuous at least between 42°S and 36°30'S, over some 500 km. Some of the submarine canyons are connected to this trench channel by a single connecting feeder channel (as

in the case of the Tolten Canyon) or by a number of distributary channels winding though the sediment fan (as in the case of the Biobio and Callecalle Canyons). The rugged terrain of the Nazca plate forms the seaward boundary of the trench. It is elevated in respect to the filled trench and shows parallel lineaments originating from horst- and graben structures. Seamount chains and elongated ridges appear to be more or less aligned parallel to the prominent fracture zones (e.g. Vema Fracture Zone). When approaching the trench, Nazca Plate seamounts become progressively buried by the trench fill.

Sedimentation

The sediment input from land is at present times mainly transported into the sea by rivers in this sector of Chile (Lamy et al., 1998). The erosion rate of the hinterland is supposed to be very high, although reliable data are scarce. The humid westerlies lead to rainfall at the western slope of the Southern Andes, resulting in precipitation rates of up to 200 cm/y (New et al., 1999) and a runoff of 100-250 mm/y (Fekete et al., 2000). The larger rivers (Biobio and Callecalle) emerge from the Southern Andes, cross the central valley of Chile and cut through the Coastal Cordillera. Tolten River partly emerges from the Coastal Cordillera. We suppose that actually the larger portion of the sediment is deposited within the Central Valley.

ODP site 1232, cored on leg 202, was drilled at the seaward limit of the sediment-filled Peru-Chile Trench (Fig. 1a). The upper 362 meter of the sediment sequence represent Pleistocene sediments and consist of gray silty clay and clay, interbedded with numerous (>800) graded layers of silty sand, partly with sharp basal contacts (Shipboard Scientific Party, in press). The silty sand layers were interpreted as basal parts of distal turbiditic deposits. They make up as much as 22% of the uppermost 20 m of the sequence and range in individual thickness from a few cm to 108 cm (Shipboard Scientific Party, in press). Both interbedded lithologies show a mineral assemblage which is consistent with andesitic source rocks of the Southern Andes. The stratigraphy of the cored sequences indicates high overall sedimentation rates (>450 m/My, possibly much higher in the upper section), resulting in a high frequency of turbidite events on the order of 1 event per 100 years. The distance of the ODP site from the lowermost continental slope (85 km) and the thickness of individual turbidite layers (>1 m) suggest large depositional events.

Oceanography near the Chilean Coast

We focus on those currents which are close enough to the shelf, slope, and trench floor to interact with downslope turbidity currents and potentially influence the sediment dispersal.

The poleward Gunther Undercurrent (or Poleward Undercurrent, PUC) at 0.2-0.5 km water depth flows close enough to the edge of the shelf to induce coast-parallel southward sediment transport. Current velocities ranging from 0.1 to 0.5 m/s at depths of 100-300 m were measured with a variety of methods (Huyer et al., 1991). Shaffer et al (1999) reported a mean value of 0.128 m/s and a maximum value of 0.689 m/s over a period of 6 years. Our sediment echosounder studies may serve as additional, albeit indirect evidence of high current velocities, as the shelf seems to be virtually free of unconsolidated sediments.

Below the Gunther Undercurrent, Antarctic Intermediate Water (AAIW) spreads northward at a depth of 0.5-1.0 km. Measured mean velocities are about 0.011 m/s (Shaffer et al., 1999).

At 1-3 km water depth, below the AAIW, the slow, poorly studied Peru-Chile Countercurrent flows as a coast-parallel southward flow (Pacific Deep Water). Sediment-echosounder data of the SONNE cruises 161-3 and 161-5 show no indication of contourites, mudwaves or other sedimentary features of the seafloor indicative of enhanced bottom water currents. This implies low bottom water velocities, probably on the order of some cm/s.

A prominent oceanographic feature of the area is the double oxygen minimum zone (OMZ) with oxygen minima at 400 m and 1500 m water depths (WOCE, 2002). These water masses, depleted in oxygen ($>150 \mu\text{mol/kg}$ water) are related to the high-productivity upwelling zones off northern Chile and Peru. They are transported from the north by the Gunther Undercurrent and the Pacific Deep Water.

Methods

The samples under discussion were obtained in 2002 during expedition SO161-5 of the German RV SONNE. The sampling tool was a standard 1.5 t gravity corer which retrieves sediment cores with a diameter of 10 cm. The cores were routinely opened and described on board.

Laser granulometry

The grain-size distribution analysis of prominent turbidite layers within the cores was performed with a liquid laser-particle analyser (Galai CIS-100). Individual beds were sampled by extracting tubes in a spatial resolution of 1 cm. Five cm^3 of fresh sediment was taken into a 100 ml PET-bottle and filled with deionised water. 1 ml of 1M NH_4 -solution was added to the suspension to prevent adhesive bonding of sediment particles. The sediment suspension was then analysed for 120 s, determining particle sizes between 0.5 and 600 μm . The interval $<10 \mu\text{m}$ was measured in steps of 1 μm , from 10 to 100 μm in steps of 10 μm , and between 100 and 600 μm in steps of 50 μm .

Components (Benthic Foraminifera, mineral assemblage)

Sediment samples of turbiditic layers were wet-sieved over a 63 µm sieve. Foraminifera were picked from the >125 µm fraction and mounted on EM-carriers for photographic documentation with a Zeiss Scanning Electron Microscope (DSM 960 A). The benthic foraminifera were then identified by comparison with publications covering the Peru-Chile Trench area (Bandy & Rodolfo, 1964; Ingle et al., 1980). As certain species are characteristic of different environments (e.g. dissolved oxygen, temperature) they can be related to water masses and respective water depths. The mineral assemblage was examined by thin sections of grain mounts. The fresh sediment material was wet-sieved with a 63 µm sieve and washed with deionised water. The residual sediment was dried at 60° for 24 hours. Each sample was then fixed with resin for the final grain mounts. The thin sections were then studied for mineral content and photographed.

Oxygen isotopes

Oxygen isotopic composition was determined using the planktonic foraminifera *G. bulloides*. The samples were extracted from the core in 10 cm intervals. We choose only those samples which were taken from background sediments avoiding typical turbiditic layers as the latter may contain misleading redeposited foram tests. Tests were treated with 100% phosphoric acid (Wachter and Hayes, 1985) at 75° C using a Kiel III online carbonate preparation line connected to a ThermoFinnigan 252 mass-spectrometer. All values are reported in per mil (‰) relative to V-PDB. Reproducibility was checked by replicate analysis of laboratory standards ($\delta^{18}\text{O}$ $1\sigma < 0.08\text{\textperthousand}$). The resulting curves were then graphically correlated with marine standard oxygen isotope curves (Martinson et al., 1987).

Sediment echosounding with the Parasound System

Along the track of RV SONNE cruises 161-3 and 161-5, sediment echography was performed with the hull-mounted parametric sediment echosounder PARASOUND (Krupp Atlas Elektronik). The PARASOUND echosounder makes use of the acoustic nonlinear properties of the water (the parametric effect) to generate a signal in the range of 3.5 to 5.5 kHz with a narrow opening angle. This focussed signal results in a comparatively small signal footprint at the seafloor with a diameter of about 7 % of the water depth. Thus, the lateral and vertical resolution is significantly improved in comparison with conventional 3.5 kHz echosounding systems. The major drawback of the focussing of the acoustic energy is the signal reflection to the sides where inclination of the seafloor exceeds some degrees. Consequently, good profiles were obtained on the shelf and in the deep

sediment-filled graben and on the Nazca Plate, whereas on the continental slope only some small intraslope basins provided useable records. PARASOUND data were digitized and recorded with the data acquisition system PARADIGMA (Spiess, 1993) for further processing and plotting. The profiles produced by PARASOUND image the shallow subsurface to a depth of 30 to 100 m (depending on sediment composition). This allows for the interpretation and mapping of sedimentation and redeposition processes in the upper sediment column. Furthermore, the overall impression of the energy return (echo character) provides clues to the sediment composition, and allows to discriminate different styles of sedimentation.

Swath Bathymetry

During SONNE cruise legs 161-1 to 161-5, the KONGSBERG SIMRAD EM 120 multibeam echosounder was operated continuously. The EM 120 system enables mapping of the seafloor from shelf to deep sea with high resolution and accuracy. The signal frequency is 12 kHz. Signals are emitted as an array of 191 single beams, covering a swath angle of up to 150°. The opening angle of the single beams are as narrow as 1°. The sounding rate depends on water depth with a maximum rate of about 5 Hz in shallow water.

The cruise tracks were designed to obtain maximum coverage, which resulted in a bathymetric data set of extraordinary quality and extent. The quality of the dataset acquired during leg 3 benefited from the low ship velocities of 5 kn. The regions of special interest to the topic of this paper were covered by more than one profile line.

We combined the cruise data into a bathymetric grid with the MB-System Tools software (Caress & Chayes, 1995, 1996). We applied only minimum filtering in order to preserve a maximum of microtopographical information. Editing was done by hand rather than automatically. The resulting bathymetric maps of the core location areas (figs. 1b and 1c) are based on a 200 m grid.

Results

Core description and grain size distribution

During cruise leg SO 161-3 (Wiedicke et al, 2002) three gravity cores, SL50, SL100 and SL101 (from N to S) were recovered from the summits and flanks of three unnamed seamounts which rise 200 m, 270 m and 600 m respectively from the surrounding abyssal plain of the trench fill (figs. 2a and 2b). The seamounts are isolated bathymetric features 13 km, 25 km and 30 km away from the foot of the Chilean continental margin.

The cores sampled 7.32 m (SL50), 3.90 m (SL100) and 3.28 m (SL101) of the seamount sediment sequence. The sampled material was classified as clayey mud, muddy clay and muddy pelletal sands grading into silty clay interbedded with numerous thin graded black sand layers (Wiedicke et al., 2002). The sand layers have sharp bottom contacts, are massive or partly laminated and can be macroscopically identified by their dark colour and coarse composition.

The coring site of SL50 lies on top of a small, elongate seamount which rises 200 m from the surrounding abyssal plain. The site is 13 km away from the foot of the continental slope (Fig. 2b). We counted 36 individual turbidite layers within core SL50. Most have a thickness of 1 to 4 cm, whereas two exceptional beds are found in the depth intervals 037-042 cm and 054-059 cm. These stand out visually because of their thickness, darkness, and comparatively large grain size (Fig. 3, table 1) with about half of all grains measuring $>100 \mu\text{m}$. Interval 037-042 cm of core SL50 contains as much as 36.9 volume % of grains in the size range 100-150 μm and 18.25 volume % of grains within the range of 150-200 μm at 039 cm core depth (Fig. 3, table 1). Interval 054-059 cm of core SL50 contains as much as 32.31 volume % of grains in the size range 100-150 μm and 17.46 volume % of grains within the range of 150-200 μm at 058 cm core depth (Fig. 3, table 1). This is in sharp contrast with the pelagic background sedimentation which shows its maximum of 26.1 % in the interval 10-20 μm .

The coring site of SL100 is situated on top of a cone-shaped seamount which rises 270 m from the surrounding abyssal plain. It lies directly landward of the axial channel which winds around its foot (Fig. 2c). The site is 25 km off the lower slope. We recognized some thicker individual turbidite beds and a set of thin turbidite beds which were homogenized by bioturbation within core SL100. We sampled the most prominent beds at the depth intervals of 304-306 cm, 338-341 cm, 350-352 cm and 370 cm. The grain-size analysis of those beds show that they consist mainly of coarse silt. Thus, they are much finer grained and thereby less distinct from the pelagic background sedimentation than the turbidite layers of core SL50.

The coring site of SL101 lies within a horseshoe-shaped depression of a third seamount. The northern rim of the crater rises 600 m from the surrounding abyssal plain. The coring site is elevated 150 m in respect to the abyssal plain seaward of the seamount and 300 m in respect to the floor of the axial channel (Fig. 2c). Immediately east (on the landward side) of the seamount lies the intersection of the axial channel and a wide linear depression originating at the Tolten Canyon exit (Fig. 2). The coring site is 25 km away from the lower slope of the Chilean margin. Core SL101 exhibited black sandy beds at the depth intervals of 120-131 cm, 228-232 cm, 290-292 cm and 309-310 cm as well as some minor discontinuous black sand layers. The thick turbidite layer in the 120-131 cm interval is less well marked by sand content but has a higher density as is recorded

by a sharp drop in the Gamma Ray Core Log. The bed of the interval 228-233 cm shows a plane-parallel (tb-) bedding and a sharp contact at the base. The lowermost part of the turbidite contains abundant fine sand (33.97 volume-% in the range 100-150 μm).

The most prominent beds by thickness and grain size are intervals 037-042 cm and 054-058 cm in core SL50 and 228-233 cm in core SL101. Less prominent in terms of elevated median grain size but conspicuous by its thickness is interval 120-132 cm in SL101.

The grain size distribution of the sampled layers proves grading of the massive beds. In the interval 037-042 cm of core SL50, the cumulative percentile value of 50 % or median, D_{50} , increases downcore from the top of the bed at 037 cm to a maximum at 039 cm and decreases further downcore (see figs. 3a, 3b). The maximum value of D_{50} is 110 μm . The basal contact of the bed, which is observed visually is less clearly represented by the data, maybe due to bioturbation. The background sedimentation is represented by the cumulative grain size curve at 042 cm depth (D_{50} value 18 μm).

The interval 054-058 cm shows a constant downcore increase of D_{50} from 55 μm to 105 μm . The basal layer contains 32.3 volume percent grains in the range 100-150 μm .

The interval 120-132 cm in SL101 is a thick, rather uniform layer. It is well visibly coarser than the background sedimentation above and below, but not as coarse as interval 227-233 cm. Grading is indicated by a downcore trend in median grain size from 30 μm to 55 μm but not continuous.

In the interval 227-233cm of SL101 grading is clearer (figs. 3c, 3d). The median of the samples increases downcore from the top of the bed (227 cm depth, 25 μm mean grain size) to the base of the layer (232 cm depth, 100 μm mean grain size, figs. 3c, 3d). The sharp basal contact of the bed is shown by the sudden drop of the mean grain size to about 15 μm below (233 cm), which represents the background sedimentation.

We subsampled material of the named layers in core SL50 for further investigations of the nature of the causing events.

Mineralogy of core SL50

Benthic foraminifera in core SL50

The samples of the turbidite layers of core SL50 contain few, but diagnostically significant benthic and planktonic foraminifera (Fig. 4). We use the established relationship between water depth and/or dissolved oxygen concentrations and the relative abundances of several species of benthic foraminifera in sedimentary environments to determine the primary depositional depths of the reworked components (e.g. Bernhard, 1986; Ingle et al., 1980; Kaiho, 1991; Kaiho, 1994; Schmiedl

et al., 1998). The composition of benthic foraminifera assemblages varies, but many contain shallow water species.

Typical representatives of the outer-shelf biofacies (135 – 150 m water depth) are *Nonion Mexicanum* (Williamson), *Cassidulina Sp.* and *Trifarina Angulosa* (Williamson, Fig. 4). In particular *Cassidulina Minuta* is typical for the shallow oxygen-minimum fauna (~1.5 ml/l) of the continental margin of Chile (Ingle et al., 1980).

Globobulimina Affinis (d'Orbigny) and *Uvigerina Peregrina* (Cushman) are members of the upper bathyal biofacies (Ingle et al., 1980) and are associated with dissolved oxygen contents lower than ~3 ml/l and a depth-distribution between 150 and 500 m.

Uvigerina Hispida (Schwager) is typical and abundant in sediments from water depths between 500 to 1500 m. Off Chile this water depth range comprises an oxygen-rich upper part (500 – 900 m, the Antarctic Intermediate Water) and a oxygen-depleted lower part (900-1500 m). *Uvigerina Hispida* (Schwager) is characteristic for the latter.

The lower middle bathyal biofacies (1500-2000 m water depth) is represented by *Bulimina Barbata* (Cushman), one of the index species for this depth (Ingle et al., 1980).

In summary, the benthic foraminifera in samples represent a mixed fauna, which cannot be related to an in-situ community of a water depth at~4000 m. The abundance of *Cassidulina Sp.*, and *Uvigerina Hispida* (Schwager) is definitely a signal for oxygen-deficient water conditions, which do not prevail at the sampling sites.

Age of turbidites in SL50

Most of the core SL50, from the base to 1.5 m core depth, exhibit a relatively uniform and fairly “heavy” oxygen isotope signal in the range of 2.5 - 3.5 ‰ (Fig. 4). This pattern can be related to the last glacial period (MIS2). From 1.5 m core depth to the top of the core there is a sharp decrease of $\delta^{18}\text{O}$ values from 3.0 ‰ to 0.7 ‰. This event is interpreted to represent the global warming of the atmosphere after the last glaciation and is very similar to the much higher resolving $\delta^{18}\text{O}$ curve derived from the Vostok ice cores (Bender, 2002). The topmost 30 cm of the core SL50 represent the Holocene. The thin Holocene section and the more than 5 m (minimum) thickness of the Glacial section suggest, that sedimentation rates were significantly higher during the Glacial than during the Holocene time period. The two thick turbidite layers described above fall into the transition period between Glacial and Holocene and are about 8-13 ky old.

Sediment distribution in the vicinity of the coring sites (PARASOUND, SIMRAD)

High resolution sediment echosounder (Parasound) profiling across the trench show few easily distinguishable echo patterns. Their appearance and distribution is fairly uniform indicating a low variability of basic sediment types and modes of sedimentation. West of a widespread chain of trench-parallel foothills at the base of the continental slope, profiles show low signal penetration and indistinct energy return. This acoustic character is produced by a high number of flat-lying, semi-parallel, densely spaced internal reflectors which are continuous for several kilometers (fig. 6a, echotype A). The topographic gradient of the trench fill is very low with the exception of the axial channel and the fan systems and distributary channels related to the submarine canyon systems of Tolten and Biobio. The axial channel cuts up to 150 m deep into the sediments, truncating reflectors at the channel walls. There is no systematic difference in the height of both of the shoulders of the axial channel. We found no indication of sediment waves or drift sediments which could be interpreted in terms of bottom water currents in trench.

The seaward limit of the flat trench fill is marked by the fairly rough topography of the Nazca Plate. Its surface displays a characteristic linear topographic pattern caused by the crustal horst- and graben structure which is masked only by a relatively thin hemipelagic cover. Acoustically, this cover is characterized by evenly spaced, continuous and very distinct reflectors (fig. 6b, echotype B). These reflectors are parallel to each other follow the undulating seafloor surface. The signal penetration is significantly higher than within the trench sediments. The transition between both facies takes place at a defined height of 200 m above mean trench depth and 350 m above the floor of the axial channel. Seismic images show that the transition is time transgressive as is indicated by the progressive onlap of the horizontally stratified turbiditic trench sequence on the pelagic drape of the incoming Nazca Plate.

Discussion

The graded layers which we encountered at topographic highs within the trench were deposited by turbidity currents. This interpretation is based on the sedimentary structures and the composition of the layers: sharp bottom contact, graded bedding, mixed benthic foram assemblages including upper and lower slope species. Additionally, the coarser components of these layers mainly consist of volcanic rock fragments which have a mineralogy with a close affinity to the alkaline volcanites of the Andean hinterland.

The deeply incised canyons provide major potential pathways for the downslope sediment transport of such turbidity currents. However, the mixture of components of various depths of the entire continental slope clearly shows, that significant amounts of sediment of all slope sections have been incorporated into individual turbidite layers. A local slope failure e.g. at the upper slope most likely generates a turbidity current confined to the incised canyon; it is unlikely to supply such a diversity of components to the turbidity current and to generate a turbidite layer within the trench as described above (xx). We think this is an argument in favor of large events which mobilize sediments from extended slope areas, thus, providing components from a broad variety of environments and depths.

A second argument for the large size of at least some of these turbiditic events is the position of the sampling sites 200 m, 270 m and 600 m above the trench floor. Site 100SL, 270 m above the trench, displays a fairly fine-grained size spectrum (silty) of the turbidite layers, which we consider as very distal in character; site 50SL, 200 m above the trench, shows a more pronounced turbiditic impact as can be seen in its numerous sandy layers.

To determine the upper reach of the turbiditic depositional environment we have used the seismic character of the sediments on our Parasound profiles across the trench: echotype A (Fig. 6A) is typical for the trench sediments with a relatively high content of silt and sand in thin beds, most probably representing distal turbidites. Echotype B (Fig. 6B) was found at the area of the hilly topography of the incoming Nazca Plate with a predominantly (hemi)pelagic sediment cover. It monitors sedimentation processes which are independent of the seafloor topography, as younger reflectors mimic the shape of the preceding deposits (sediment drapes).

The transition from echotypes A to B (shown as dashed line in fig. 1a) thus delimits the average westward and upward turbiditic depositional environment. According to the position of this line, turbidites spill out into the trench and cross the axial channel. After travelling over essentially flat ground for 50-80 km they climb the bulging Nazca plate covering an elevation difference of 350 m. Neither bathymetry nor reflection character of the trench fill support a substantial role of the axial channel in dividing areas, different in sedimentation rate and sediment type. If the axial channel formed an obstacle to the westward motion of the turbidites, it would separate areas covered by turbidites from such which are not, or at least produce some kind of grain-size sorting on the respective sides. The seismic reflection character suggests that turbidites cross this 200 m deep feature frequently. This can be accomplished either by transverse (E-W) transport, or, alternatively, by major overbank-spilling during northward transport in the axial channel.

The position of the three samples allows to differentiate these two possibilities: Core site SL50 lies close to the lower slope of the continental margin, well away from the axial channel and distant

from major canyon mouths (fig. 1b). Its thick turbidite bed may therefore be due to single, large, unchannelized events.

Sites SL100 and SL101, in contrast, are situated just a few km north of the junction of the Tolten Canyon mouth with the axial channel winding between them (fig. 1c). The turbidites are therefore generated by flows channelized within the axial channel. This interpretation is also supported by the observation of large-scale scouring on the axial channel opposite the mouth of the Tolten fan feeding channel (Fig. 1c, dashed arrow) Material coming down the Tolten Canyon apparently enters the axial channel and partly turns northwards. Another part shoots across the channel by its momentum and erodes the western bank of the axial channel. During larger events of this type, silt-sized material washes into the crater of the seamount and is deposited here. We propose that the graded layers within core SL101 are overbank deposits on the outer bank of a northward-turning, large turbulent cloud, leaving the Tolten Canyon Fan.

SL100, finally, situated 17 km downstream receives sediments from northward-travelling turbidity currents where the axial channel causes overbank deposits as it turns NNW.

References

- Bandy, O. L., and K. S. Rodolfo (1964). Distribution of foraminifera and sediments, Peru-Chile Trench Area. Deep-Sea Research 11: 817-837.
- Bangs XX and XX Cande (1997). Episodic development of a convergent margin inferred from structures and processes along the southern Chile margin. Tectonics, 16: 489-503
- Bender, M. (2002). Concentration and isotopic composition of O₂ and N₂ in trapped gases of the Vostok ice core. Boulder, CO: National Snow and Ice Data Center. Digital media
- Bernhard, J.M. (1986). Characteristic assemblages and morphologies of benthic foraminifera from anoxic, organic-rich deposits: Jurassic through Holocene. Journal of Foraminiferal Research, 16: 207-215.
- Caress, D. W., and D. N. Chayes (1995). New software for processing sidescan data from sidescan-capable multibeam sonars, Proceedings of the IEEE Oceans 95 Conference, 997-1000.
- Caress, D. W., and D. N. Chayes (1996). Improved processing of Hydrosweep DS multibeam data on the R/V Maurice Ewing, Mar. Geophys. Res., 18, 631-650.
- Emiliani, C. (1955). Pleistocene Temperatures Journal of Geology 63: 538-578
- Fekete B. M., Vörösmarty, C. J., and W. Grabs (2000). Global Composite Runoff Fields Based on Observed River Discharge and Simulated Water Balances. Complex Systems Research Center, University of New Hampshire. UNH-GRDC Composite Runoff Fields v1.0. <http://www.grdc.sr.unh.edu> (version of 15.05.04)
- Huyer A., Knoll, M., Palusziewicz, T., and R. Smith (1991). The Peru undercurrent: a study of variability. Deep-Sea Res., 38: 1-38.
- Ingle, J. C., Keller, G., and R. L. Kolpack (1980). Benthic foraminiferal biofacies, sediments and water masses of the southern Peru-Chile Trench area, southeastern Pacific Ocean. Micropaleontology, 26(2): 113-150.
- Kaiho, K. (1991). Global changes of Paleogene aerobic/anaerobic benthic foraminifera and deep-sea circulation. Palaeography, Palaeoclimatology, Palaeoecology, 83: 65-85.
- Kaiho, K. (1994). Benthic foraminiferal dissolved-oxygen index and dissolved-oxygen levels in the modern ocean. Geology, 22: 719-722.

- Lamy, F., and D. Hebbeln (1998). Terrigenous sediment supply along the Chilean continental margin: modern regional patterns of texture and composition. *Geologische Rundschau* 87: 477-494.
- Martinson et al. (1987). Age Dating and the Orbital Theory of the Ice Ages - Development of a High-Resolution-0 to 300,000-Year Chronostratigraphy. *Quaternary Research*, 27(1): 1-29.
- New, M. G., Hulme, M., and P. D. Jones (1999). Representing 20th century space-time climate variability. I: Development of a 1961-1990 mean monthly terrestrial climatology. *J. Climate*. 12, 829-856.
- Pizarro, O., Shaffer, G., Dewitte, B., and M. Ramos (2002). Dynamics of seasonal and interannual variability of the Peru-Chile Undercurrent. *Geophysical Research Letters*. 29(12), 10.1029/ 2002GL 014790
- Reichert, C., and SPOC Scientific Shipboard Party Leg-2/3. (2002). Subduction processes off Chile: preliminary geophysical results of SONNE cruise SO-161(2+3). In: European Geophysical Society, XXVII General Assembly, Nice, France.
- Schmiedl, G., Hemleben, C., Keller, J., and Segl, M. (1998). Impact of climatic changes on the benthic foraminiferal fauna in the Ionian Sea during the last 330,000 years. *Paleoceanography*, 13: 447-458.
- Shaffer G., Salinas, S., Pizarro, O., Vega, A., and S. Hormazábal (1995). Currents in the deep ocean off Chile. *Deep-Sea Research*, 42, 425-436.
- Shaffer G., Pizarro, O., Djurfeldt, L., Salinas, S., and J. Ruttlant (1997). Circulation and low frequency variability near the Chile coast: Remotely-forced fluctuations during the 1991-1992 El Niño. *Journal of Physical Oceanography*, 27, 217-235.
- Shaffer, G., Hormazábal, S., Pizarro,O., and S. Salinas (1999). Seasonal and interannual variability of currents and temperature off central Chile. *Journal of Geophysical Research*, 104, 29951-29961.
- Shipboard Scientific Party (in press). Site 1232. In Mix, A.C., Tiedemann, R., Blum, P., et al., Proc. ODP, Init. Repts., 202 [Online]. Available from World Wide Web: <http://www-odp.tamu.edu/publications/202_IR/chap_03/chap_03.htm>. [Cited 2003-11-12]
- Spieß, V. (1993). Digitale Sedimentechographie - Neue Wege zu einer hochauflösenden Akustostratigraphie. Berichte, Fachbereich Geowissenschaften, Universität Bremen, 35, 199 S. (Habilitationsschrift).
- Strub, T., and J. Mesias (1998). Coastal ocean circulation off western South America. Coastal segment. In: *The Sea*. A. Robinson and K Brink. New York, Wiley. 11: 273-313.
- Thornburg, T. M., and L. D. Kulm (1990). Submarine-fan development in the southern Chile Trench: A dynamic interplay of tectonics and sedimentation. *Geological Society of America Bulletin* 102: 1658-1680.
- Wachter, E., and J. M. Hayes (1985). Exchange of oxygen isotopes in carbon-dioxide - phosphoric acid systems *Chemical Geology* 52: 365-374
- Wiedicke, M., and shipboard party (2002). Cruise Report of SONNE cruise 161-5, Bundesamt für Geologie und Rohstoffe Hannover.
- WOCE (2002) WOCE Global Data, Version 3.0, WOCE International Project Office, WOCE Report No. 180/02, Southampton, UK

Figures and figure captions

Figure 1: a) basic bathymetry and morphology of the continental margin and Peru-Chile Trench off southern Chile (36°S-40°S). The bathymetry of the slope was compiled from swath sounder data. Overlain is the seaward limit of continental margin and the seaward limit of the turbiditic infill of the trench. The latter was extrapolated from sediment-echosounder survey data. Positions of detail maps b) and c), gravity core stations and depth profiles of figure 2 are indicated. b) detail map of the vicinity of gravity core SL50. c) detail map of the vicinity of gravity cores SL100 and SL101. White arrows indicate inferred sediment transport direction. (*file: fig1_general_map.cdr*).

Figure 2: Depth profiles perpendicular to the Chilean coast (positions indicated in fig.1). Data compiled from swath bathymetric data of SONNE cruises 161-3 and 161-5 (*file: fig2_profiles.cdr*)

Figure 3: Cumulative grain-size distribution within prominent turbiditic layers of gravity cores SL50 and SL101. The samples show a steady increase in medium grain size from the overlying background sedimentation to the basis of the turbidites (*file: fig3_grainsize.cdr*)

Figure 4: Foraminifera species within the basal layer of turbidite bed layer within core SL50 (037-042 cm bsf). The different species are related to certain depth ranges and oxygen concentration ranges, as discussed in text.

- 1) *Cassidulina minuta*; Cushman, 1933, Cushman Lab. Foram. Res., Contr., Vol. 9, pt. 4, p. 92. pl. 10, fig.3
 - 2) *Nonion mexicanum*; Williamson = Nonion turgidus; Williamson, avr. Mexicanus Cole, 1927, Bull. Amer. Pal. Vol. 14, No. 51, p. 23, pl. 2, fig.11.
 - 3) *Trifarina angulosa* Williamson, 1858, Recent foraminifera of Great Britiain, Royal Soc., London, p.67, pl. 5, fig. 140.
 - 4) *Uvigerina peregrina*; Cushman, 1923, US. Nat. Mus. Bull., No. 104, 166, xlvi, 7-10.
 - 5) *Globobulimina affinis d'Orbigny* = Bulimina affinis D'Orbigny ; 1839, in de la Sagra, Hist. Phys. Pol. Nat. I'le Cuba, Foraminifères, p.105, pl.2, fig.25-26.
 - 6) *Uvigerina hisipida*; Schwager, 1866, Novara-Exped., Geol., Theil., Vol. 2, pt. 2, p. 249, pl. 7, fig. 95.
 - 7) *Bulimina barbata*; Cushman, 1927, Calif. Univ. Scripps Inst. Oceanogr., Bull., Techn. Ser., Vol..1, no.10, p.151, pl.2, fig.11.
- . (*file: fig4_foraminifera.cdr*)

Figure 5: Correlation of oxygen isotope data of benthic foraminifera of core SL50 with standard oxygen isotope curve (Vostok ice core, Bender, 2002) (*file: fig5_isotopes.cdr*)

Figure 6: Parasound-echosounder profiles from the Peru-Chile Trench and Nazca Plate. a) Image of sediments on the Nazca Plate seawards of the Peru-Chile Trench. Undulating parallel reflectors indicate sediment beds of uniform thickness (pelagic drapes). The signal penetration reaches 50 m (echotype A). b) Profile located within the trench fill. The trench floor as well as subbottom reflectors are generally horizontal-lying. Densely spaced sub-parallel reflectors give an indistinct energy return to a depth of no more than 30 m (echotype B). Both echotypes are easy to distinguish.

The seaward limit of type B and the transition to type A mark the seaward termination of continent-derived turbidites as they onlap on the pelagic strata of the Nazca Plate (*file: fig6_parasound.cdr*)

Tables

Table 1: Mineralogy of the 63 µm fraction of a turbidite layer in SL50

Depth of core	38 cm	39 cm	40 cm	41 cm
poorly sorted, fine-grained sandy siltstone	40	35	45	50
Qartz: volcanic, polycrystalline	10	15	5-10	5-10
Plagioclase	10	10	5-10	<5
Glaucnate pellets	<5	<<5	<5	<5
Volcanic Lithiclasts-andesitic	20	20	20	30
Calcite	<<5	10		
Calcite (fossile fragments, including forams)	<5	<5	<5	<5
Mmc qaurtz-sericite schist	10	10	<5	<<5
Krp	?	<<5	<5	?
Zircon	?	<<5	<5	?
Pellets, unspecified	<5	<<5	<5	5
Chert	?	?	<<5	?
Opaque	<5	<5	<<5	5
Glass	?	<<5	<<5	<<5

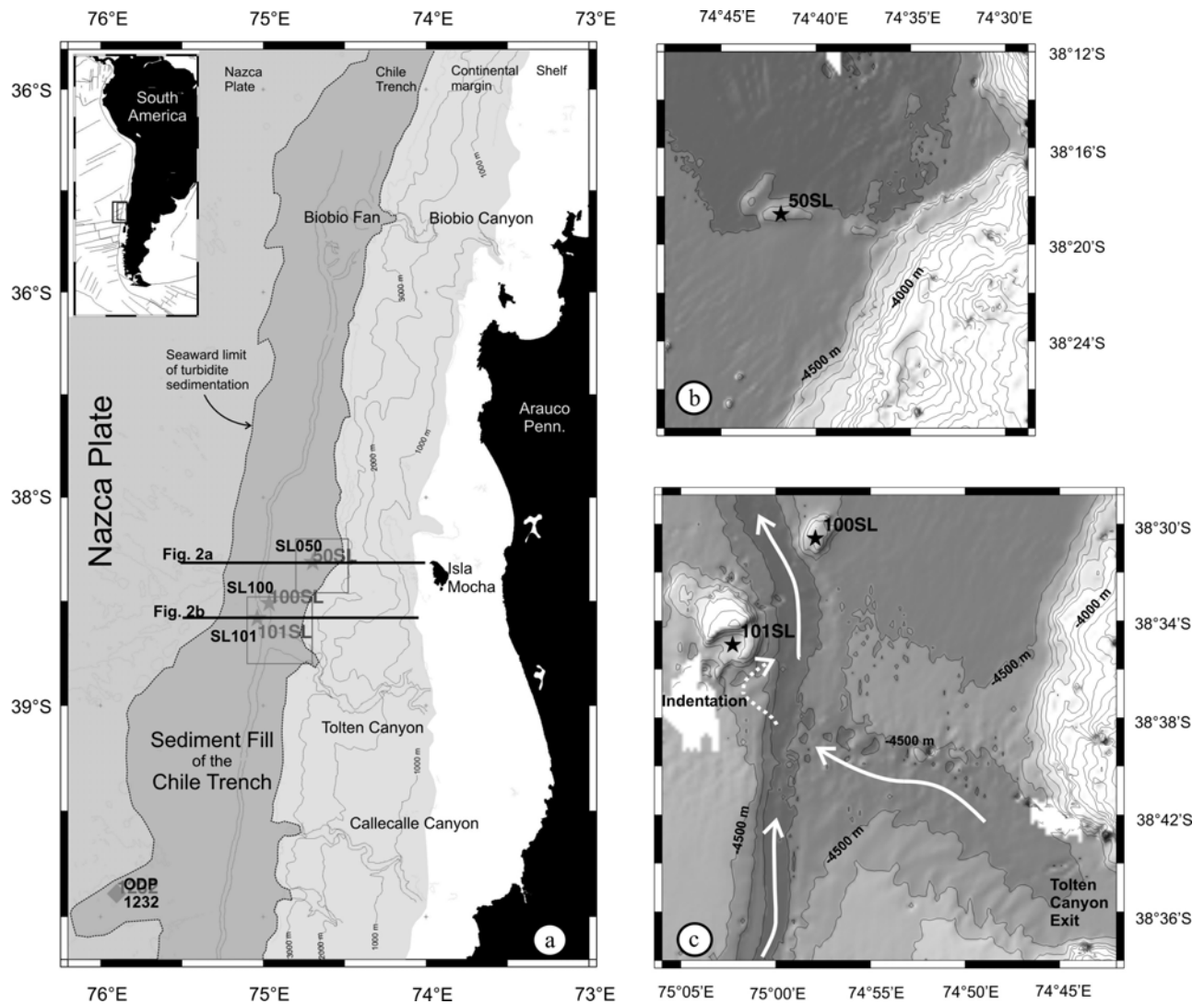


Figure 1: a) basic bathymetry and morphology of the continental margin and Peru-Chile Trench off southern Chile (36°S - 40°S). The bathymetry of the slope was compiled from swath sounder data. Overlain is the seaward limit of continental margin and the seaward limit of the turbiditic infill of the trench. The latter was extrapolated from sediment-echosounder survey data. Positions of detail maps b) and c), gravity core stations and depth profiles of figure 2 are indicated. b) detail map of the vicinity of gravity core SL50. c) detail map of the vicinity of gravity cores SL100 and SL101. White arrows indicate inferred sediment transport direction.

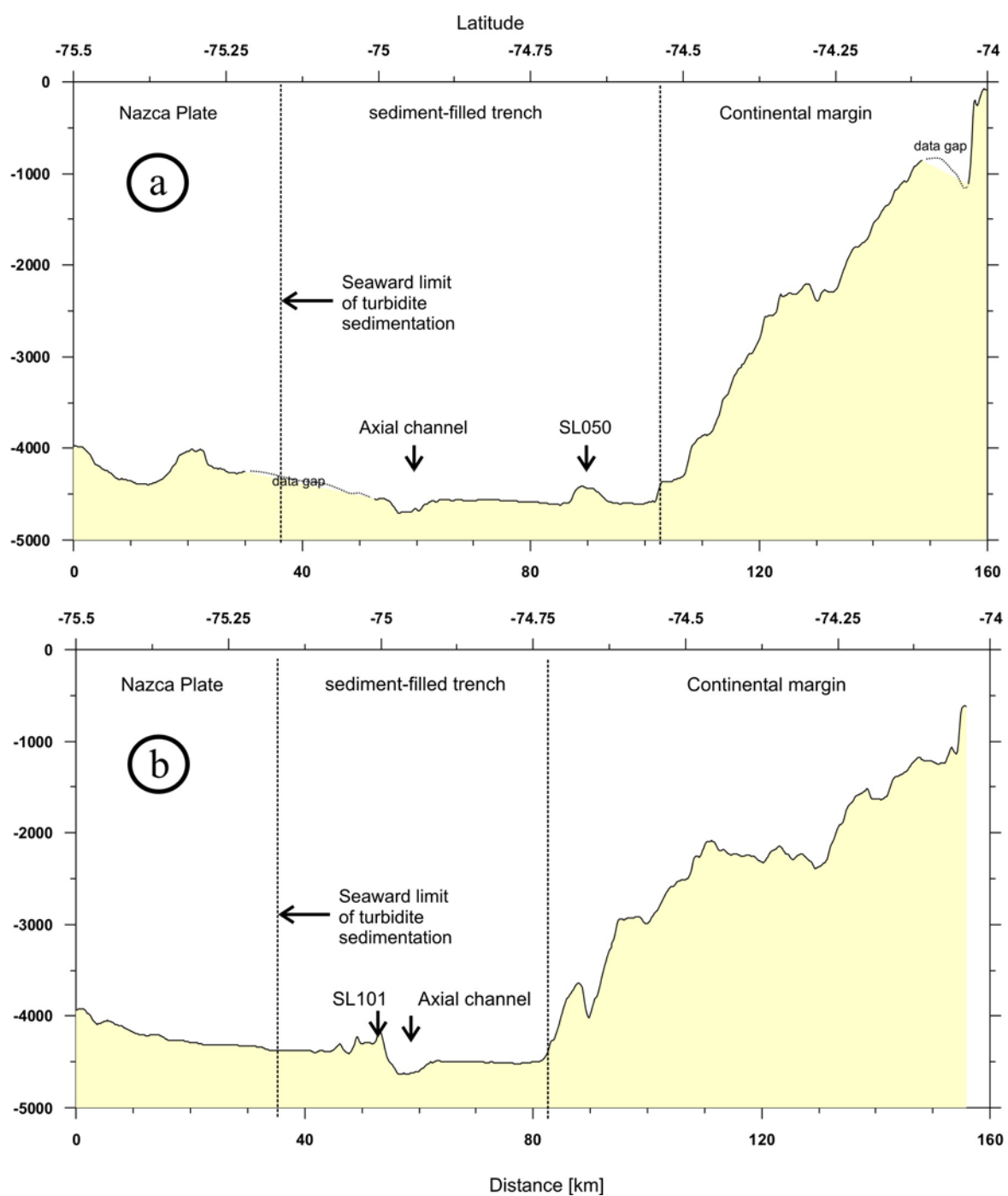


Figure 2: Depth profiles perpendicular to the Chilean coast (positions indicated in fig.1). Data compiled from swath bathymetric data of SONNE cruises 161-3 and 161-5

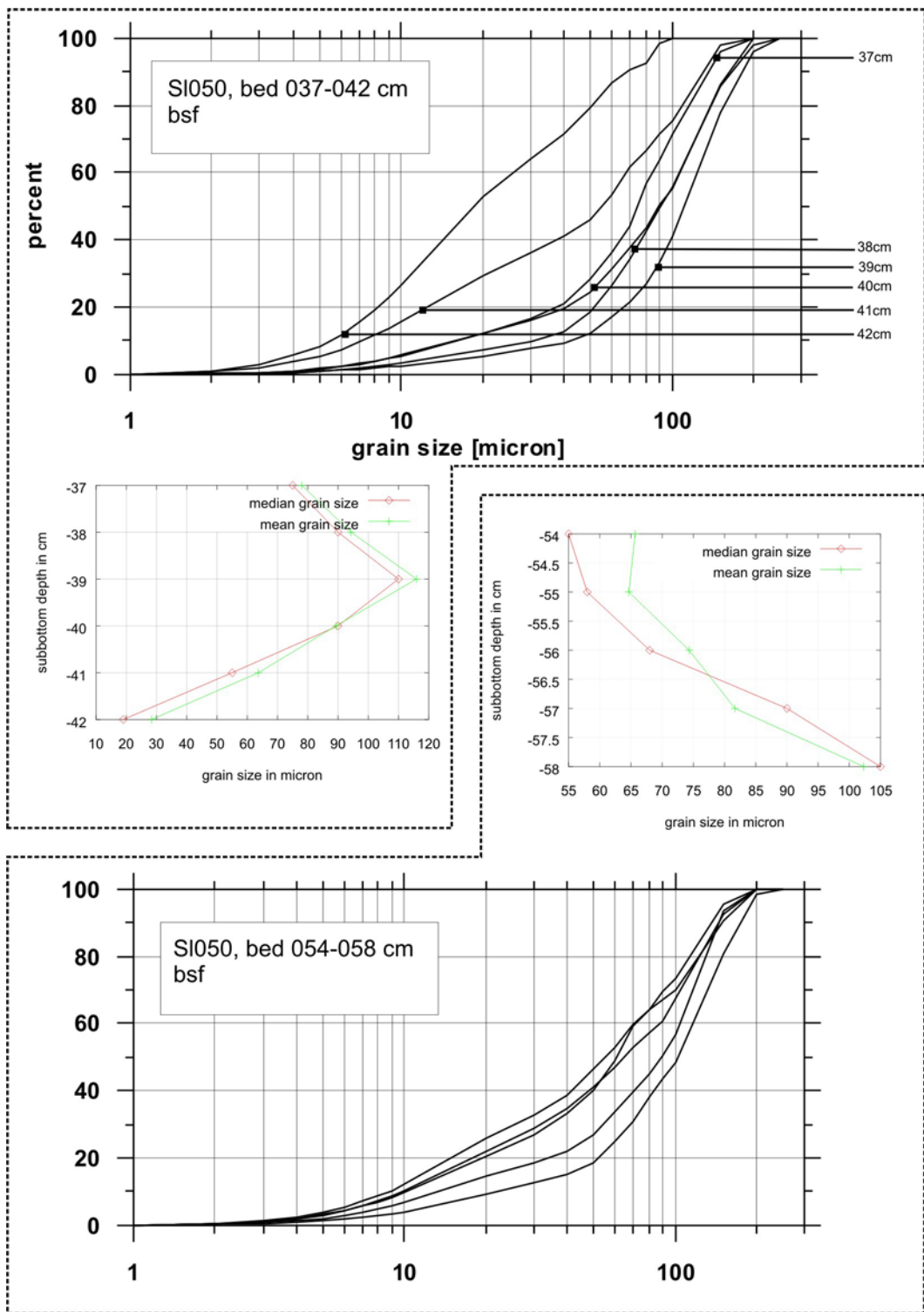


Figure 3: Cumulative grain-size distribution within prominent turbiditic layers of gravity cores SL50 and SL101. The samples show a steady increase in medium grain size from the overlying background sedimentation to the basis of the turbidites

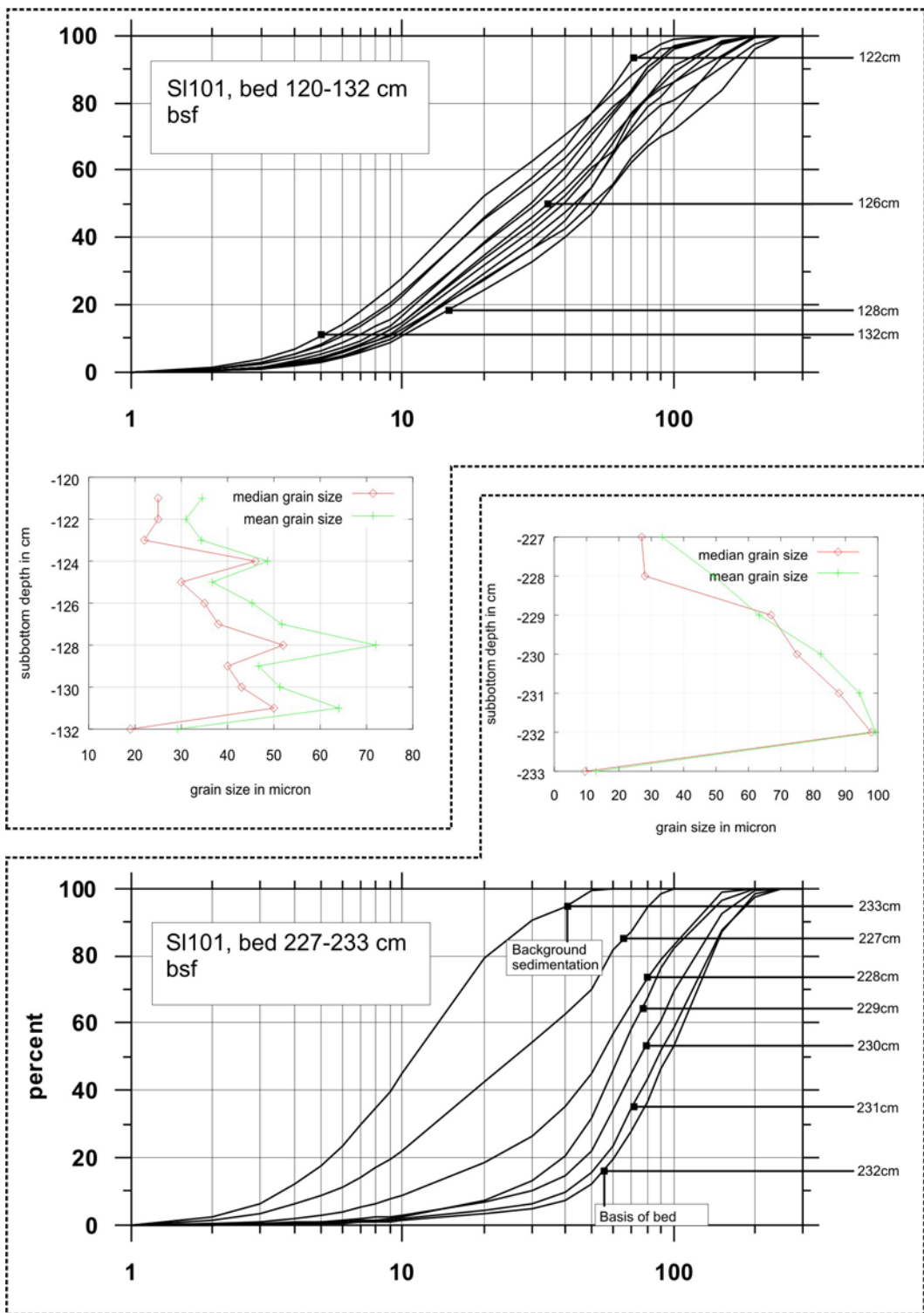


Figure 3: Cumulative grain-size distribution within prominent turbiditic layers of gravity cores SL50 and SL101. The samples show a steady increase in medium grain size from the overlying background sedimentation to the basis of the turbidites

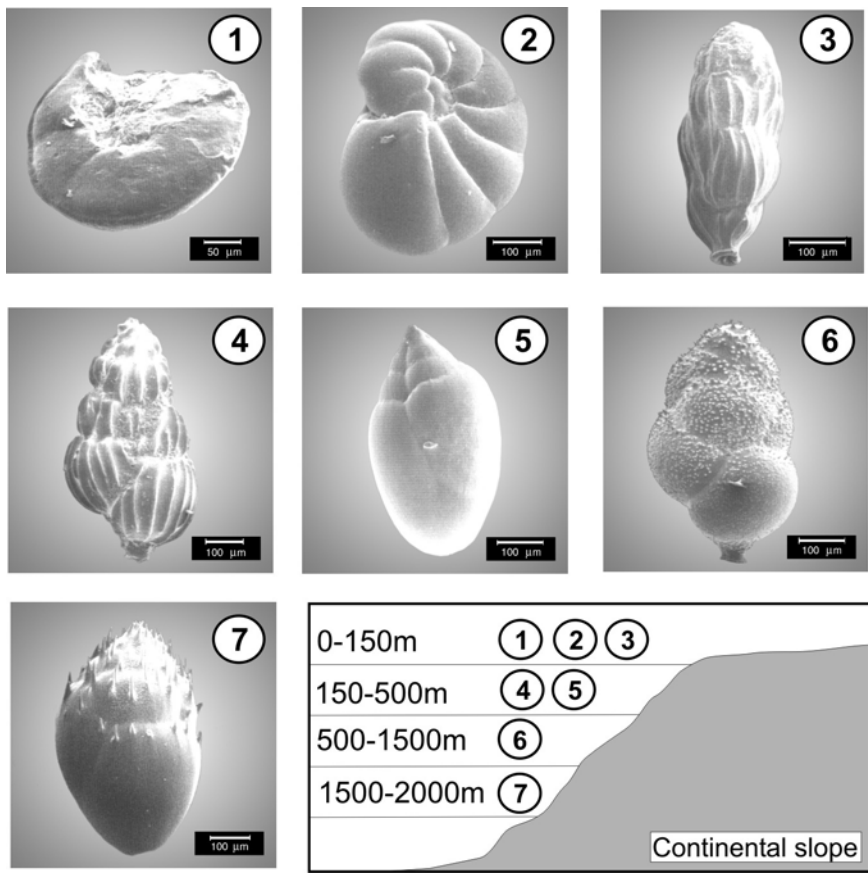


Figure 4: Foraminifera species within the basal layer of turbidite bed layer within core SL50 (037-042 cm bsf). The different species are related to certain depth ranges and oxygen concentration ranges, as discussed in text.

- 8) *Cassidulina minuta*; Cushman, 1933, Cushman Lab. Foram. Res., Contr., Vol. 9, pt. 4, p. 92. pl. 10, fig.3
- 9) *Nonion mexicanum*; Williamson = *Nonion turgidus*; Williamson, avr. Mexicanus Cole, 1927, Bull. Amer. Pal. Vol. 14, No. 51, p. 23, pl. 2, fig.11.
- 10) *Trifarina angulosa* Williamson, 1858, Recent foraminifera of Great Britiain, Royal Soc., London, p.67, pl. 5, fig. 140.
- 11) *Uvigerina peregrina*; Cushman, 1923, US. Nat. Mus. Bull., No. 104, 166, xlvi, 7-10.
- 12) *Globobulimina affinis d'Orbigny* = *Bulimina affinis* D'Orbigny ; 1839, in de la Sagra, Hist. Phys. Pol. Nat. I'le Cuba, Foraminifères, p.105, pl.2, fig.25-26.
- 13) *Uvigerina hisipida*; Schwager, 1866, Novara-Exped., Geol., Theil., Vol. 2, pt. 2, p. 249, pl. 7, fig. 95.
- 14) *Bulimina barbata*; Cushman, 1927, Calif. Univ. Scripps Inst. Oceanogr., Bull., Techn. Ser., Vol..1, no.10, p.151, pl.2, fig.11.

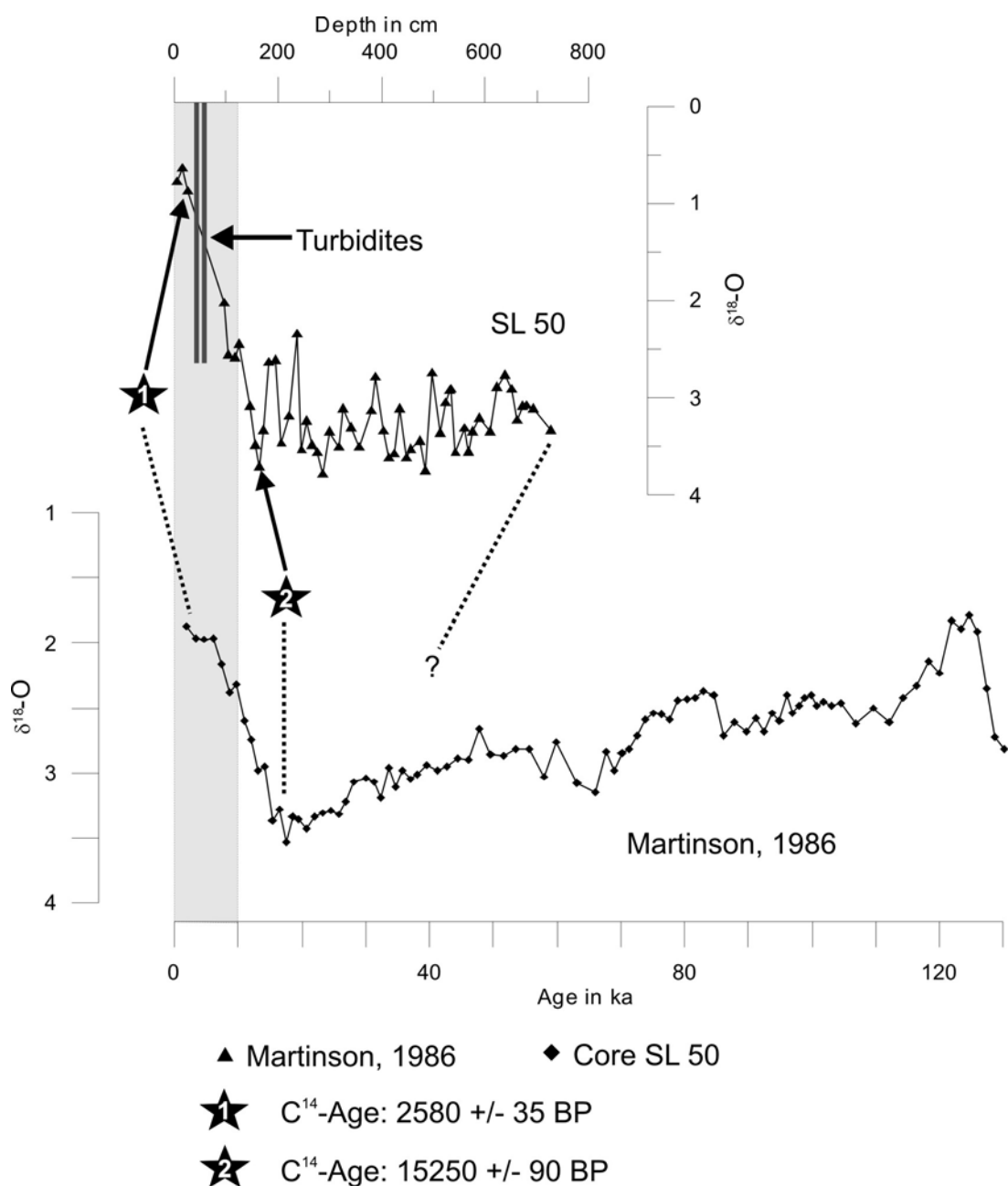


Figure 5: Correlation of oxygen isotope data of benthic foraminifera of core SL50 with standard oxygen isotope curve (Martinson, 1986)

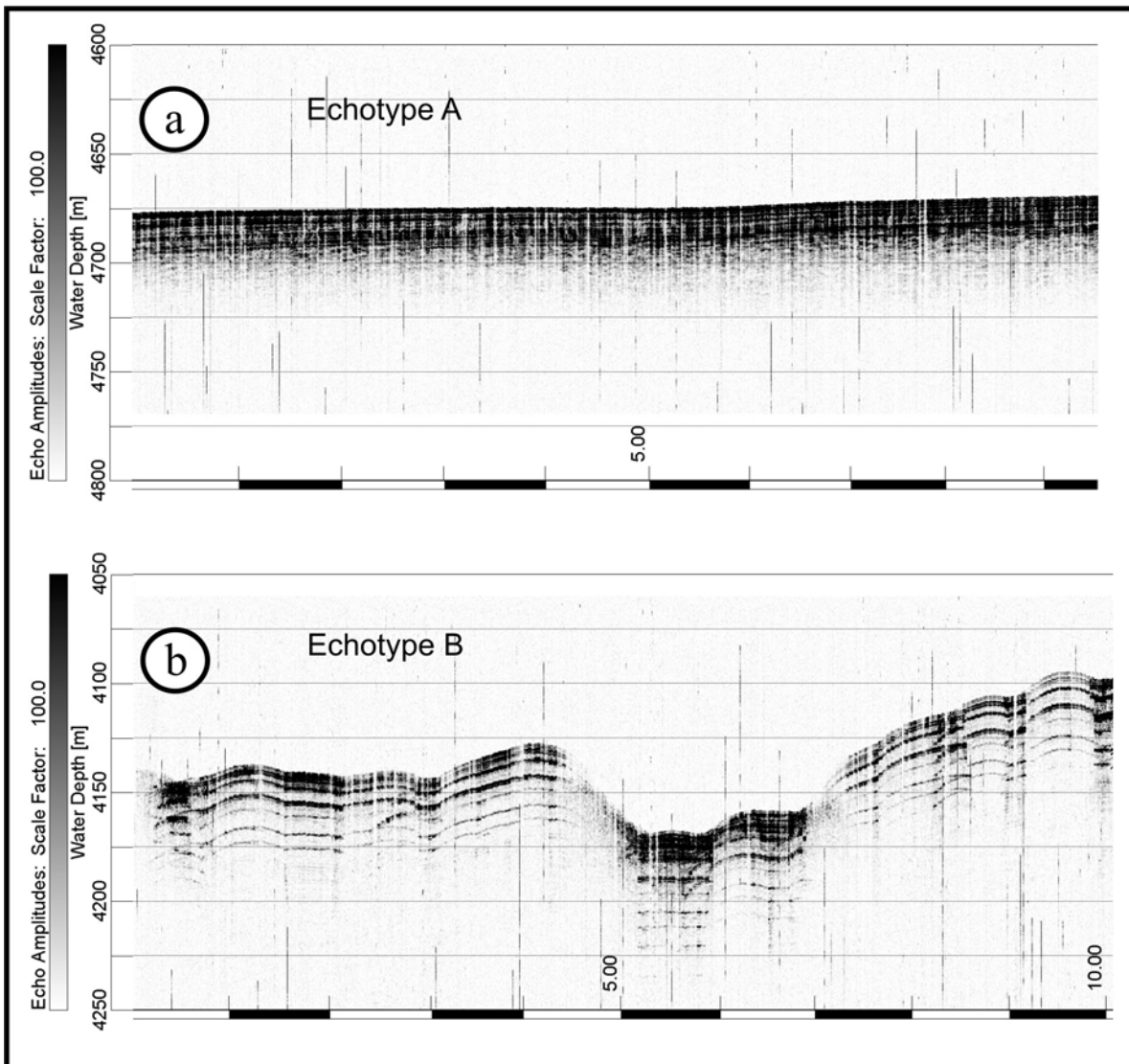


Figure 6: Parasound-echosounder profiles from the Peru-Chile Trench and Nazca Plate. a) Image of sediments on the Nazca Plate seawards of the Peru-Chile Trench. Undulating parallel reflectors indicate sediment beds of uniform thickness (pelagic drapes). The signal penetration reaches 50 m (echotype A). b) Profile located within the trench fill. The trench floor as well as subbottom reflectors are generally horizontal-lying. Densely spaced sub-parallel reflectors give an indistinct energy return to a depth of no more than 30 m (echotype B). Both echotypes are easy to distinguish. The seaward limit of type B and the transition to type A mark the seaward termination of continent-derived turbidites as they onlap on the pelagic strata of the Nazca Plate